# Towards determining the age of the Camas Prairie Ripples, NW Montana: an exercise of optically stimulated luminescence (OSL) on quartz grains

by

Quillen Michael Thornton

B.S., University of Tennessee at Chattanooga, 2024

A THESIS

submitted in partial fulfillment of the requirements for the degree

MASTER OF SCIENCE

Department of Geology
College of Arts and Sciences

KANSAS STATE UNIVERSITY
Manhattan, Kansas

2026

Approved by:

Major Professor
Dr. Joel Spencer

# Abstract

The Camas Prairie Ripples located in northwestern Montana were originally hypothesized by Joseph Pardee in 1942 to be the result of glacial outburst flooding from Glacial Lake Missoula. Despite the chronology of flood deposits in the Channeled Scablands being well studied, the Camas Prairie Ripples, which have been previously classified based on their morphology as dune and antidune structures, have little information on the exact timing for the formation of these impressive landforms. Questions also remain as to whether these features formed in one catastrophic event or resulted from repeated ice dam failures. In this study, samples of sediment matrices within giant current ripples were collected from two different localities at varying stratigraphic depth in the Camas Prairie Basin. They were analyzed using optically stimulated luminescence on small aliquots of quartz minerals to determine the age of deposition for these features and potentially answer how many flooding events may have caused these features. It was found that ages of minerals from these features ranged from approximately 3 to 6.7 ka, which are severely underestimated potentially due to malign quartz characteristics, underlying bedrock, statistical models employed, or sampling strategy and field observation methods used in this study. However, if all ages were shifted to underestimated values equally, then there could be potential evidence for at least two separate flooding events recorded in these localities. Further use of Quaternary dating methods like optically stimulated luminescence analyses on feldspars, rock surface luminescence, and $^{10}Be/^{26}Al$ cosmogenic nuclide dating may be able to help provide more accurate ages. Examination of all this information is critical to understanding the glacial history of this region and the greater Channeled Scablands.

# Table of Contents

# List of Figures

# List of Tables

# Acknowledgements

With a project of this magnitude, it often takes a village to make it happen. First and foremost, I would like to express my sincere gratitude to my advisor, Dr. Joel Spencer, for his guidance, support, and wisdom on all aspects of this project, from field work to lab work. Dr. Spencer's wisdom and kind, helpful persona helped me to develop as a scientist, student, and person. His insights and feedback were critical in guiding my research and he has taught me all I know about luminescence analysis.

I would also like to acknowledge and thank my committee members, Dr. Huan Cui and Dr. Phil Larson, for their unwavering support, valuable expertise, and insightful feedback. I hope to continue to be collaborate and look at the complex history in this area.

I would also like to specifically thank Bode Wisti as well as Adam and Laurie Cowhig for allowing us to sample on their land and help us excavate the trenches. Without them, this research would not be possible and their enthusiasm for these features was wonderful.

I would like to express my thanks and appreciation to my peers at K-State. Particularly, Saugat Ghimrie and Teagan Daer, who helped with lab preparation and analysis on this project. The Department of Geology at K-State and my family, who have supported me at all times in my academic career. Lastly, a special thanks to my friends Logan, Caeli, Levi, James, and Wyatt whose unwavering support and friendship helped keep me going and enriched my time here at K-State.

Lastly, this project would not have been possible without the generous financial support of donors. I am indebted to K-State's Luminescence Laboratory, K-State Department of Geology, K-State College of Arts and Sciences, K-State Graduate Student Council, the Geological Society of America, and the Houston Geological Society for their generous support towards research expenses, fieldwork, and conference attendance. Without all of this support, the project would not be possible. Thank you.

# Chapter 1 - Introduction

## 1.1 Background

The Camas Prairie Ripples (Figure 1.1), located in northwestern Montana, were first originally hypothesized by Pardee (1942) to be the result of glacial outburst flooding from Glacial Lake Missoula (GLM). GLM was the product of the impoundment of the Clark Fork River by the Purcell Trench Lobe that extended off the Cordilleran Ice Sheet (CIS). Since then, studies have supported this hypothesis that the source of the floodwaters that caused the Camas Prairie Ripples is GLM (Hanson and Clague, 2016; Smith, 2006). The Camas Prairie Ripples, which are classified in terms of their morphology and very limited sedimentary evidence as dune and potential antidune structures (Lister, 1975; Lee, 2009), stand approximately 4.5 m tall, are up to 76 m wide, and can extend approximately 805 m in length in certain sections (Lee, 2009; Waltham, 2010). Despite the chronology of related flood deposits in the Channeled Scablands and GLM being relatively understood (Benito and O'Connor, 2003; Hanson et al., 2012; Hanson and Clague, 2016; Smith et al., 2018), there is little information on the exact timing for the formation of these impressive landforms, and whether they were formed in a single catastrophic flooding event or resulted from repeated ice dam failures (Hanson and Clague, 2012; Smith, 2006; Smith et al., 2022). Despite this, certain Quaternary dating methods have had some successes dating landforms of these types, specifically optically stimulated luminescence (OSL) (Kalińska et al., 2025; Hanson et al., 2012; Smith et al., 2022).

OSL is a method of dating that can be used to determine the depositional age of sediment by directly analyzing the last time that mineral grains were exposed to daylight within the past 200,000 years (Rhodes, 2011). However, there are challenges to using established OSL quartz techniques on features (i.e., acute incomplete or partial bleaching) deposited by catastrophic, high energy, turbid deep waters associated with certain geomorphic mechanisms in glacial outwash environments (e.g., see Figure 3.1 in Chapter 3). Since the Camas Prairie Ripples are hypothesized to form in these types of environments, the likelihood of sufficient daylight bleaching of mineral grains, critical to OSL dating, is unknown.


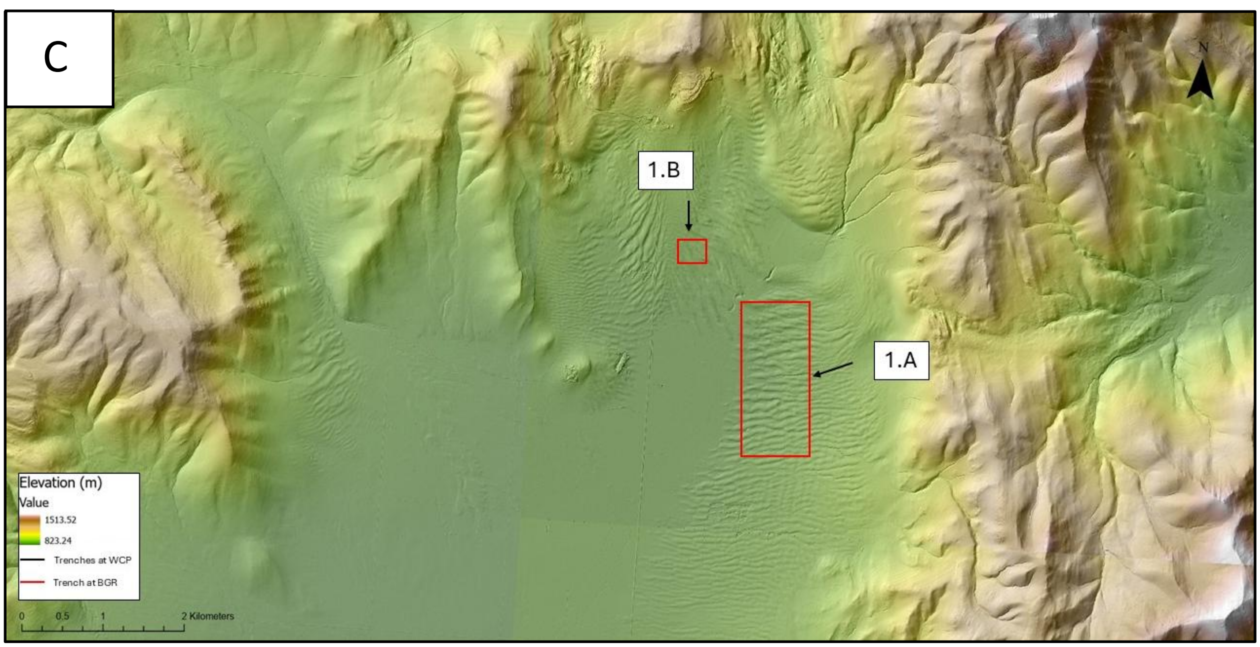


**Figure 1.1:** (A) Photo of the extent of the Camas Prairie Ripples from the top of Wills Creek Pass (WCP). (B) Photo of a section of the Camas Prairie Ripples (foreground) and Glacial Lake Missoula shorelines (background) taken from MT Highway 382. (C) LiDAR-derived DEM data,

courtesy of the State of Montana, outlining the photos of the Camas Prairie Ripples from Wills Creek Pass and MT Highway 382 on a map.

Despite this, in similar challenging environments dominated by glacial and fluvial processes, combined approaches of luminescence (including dependence on aliquot size and analysis of single grains), examination of the luminescence signal at depth within a cobble or boulder (termed rock surface luminescence), and cosmogenic nuclide dating can provide accurate chronologies to these types of features (DeLong and Arnold, 2007; Spencer and Owen, 2004; Thrasher et al., 2009). In this project, a combination of established OSL techniques on quartz sand grains was used to evaluate and characterize quartz grains from samples collected from the crests of two ripples and potentially determine a minimum age for sediment deposition.

## 1.2 Geologic History of the Camas Prairie Region

The geological history of the Camas Prairie region is very complex. Its history crosses a wide variety of geologic topics ranging from the creation of mountain belts to the growth and decay of continental ice sheets. However, each of these topics is critical to understanding the formation of the Camas Prairie Ripples, and a brief overall geologic history is provided below.

### 1.2.1 Basement Geology

The extent and glacial history of the (CIS) was heavily influenced by the regional tectonic setting as it advanced south from Canada and into the Rocky Mountain Trench (Clark et al., 2009). The Flathead and Mission Valley region of northwestern Montana is an area of active deformation that currently builds mountains through compression and extension creating valleys (Fraser et al., 2021). The Rocky Mountain Trench is not just a product of collision between the North American and Pacific plates, but also the result of the subduction of the Farallon plate under the North American plate (Hofmann et al., 2006). The valley floor of the Rocky Mountain Trench was created by extensional processes and is overprinted on top of prior compressional features (Fraser et al., 2021). One major feature located in northwestern Montana is the Mission Fault which separates the Flathead Valley to the north and the Mission Valley to the south where the study area is located. Located within the greater Rocky Mountain Trench, the Camas Prairie Basin is located in the greater Mission Valley between the Mission Mountains to the east, and the Salish Mountains to the west (Figure 1.2) (Harrison et al., 1986).

The basement geology of the region is composed of the Proterozoic Belt Supergroup which encompasses the lower Belt, Missoula Group, and Ravalli Group (Figure 1.2) (Mauk, 1983). The rocks found in these units include quartzites and argillites that were metamorphosed and deformed during the early- to mid- Cenozoic when major extension events occurred forming the valleys we currently see today (Smith, 2004). This region also houses mafic sills and dikes (ZYd, Figure 1.2) that show evidence of alteration of mafic minerals which intruded through the rocks once at ~1.4 billion years ago and again at 800 million years ago and range in thickness from less than 3 ft to 1500 ft (Harrison et al., 1986). During the late Tertiary, the rocks of the Belt Supergroup were folded and faulted due to various compressive forces that were then uncovered from erosion, revealing the bedrock seen in the Camas Prairie Basin today (Smith, 2004).

The Camas Prairie Basin is bounded on both sides by the St. Mary's Fault to the south and the Big Draw Fault to the north. To the east and west of the Camas Prairie Basin are normal faults indicated by the ball and line symbol from the resulting extensional forces that occurred in the area. Quaternary sediments are represented on the geologic map produced by Harrison et al.

(1986) as glacial, fluvioglacial, and flood deposits (Qg) which include outwash and other glaciofluvial deposits including the giant ripples that show coarse cross-bedding.

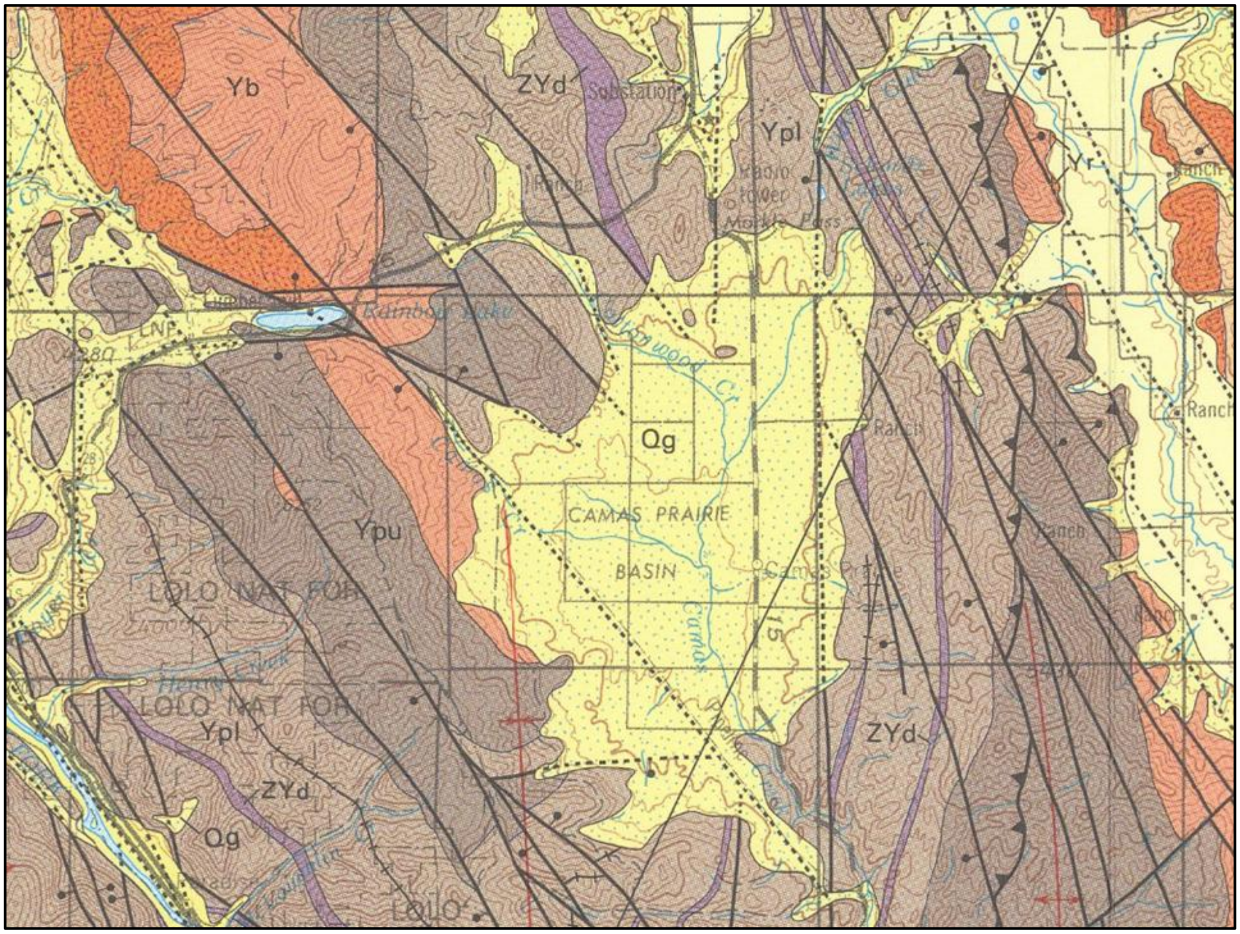


**Figure 1.2:** Section of a 1:250,000 geologic map focusing on the Camas Prairie region from Harrison et al. (1986). The different geologic map units are: Qg – Glacial, Fluvioglacial, and Flood Deposits, ZYd – Mafic Sills and Dikes, Yr – Revett Formation, Yb – Burke Formation, Ypu – Prichard Formation (upper), Ypl - Prichard Formation (lower).

### 1.2.2 Quaternary Geology

The Quaternary history of North America is a story of domination of ice on the landscape. The position of ice sheets on the continents is the ultimate driver of landscape evolution in regard to the erosion of landforms and deposition of sediment (Batchelor et al., 2019). During the last glacial period, the North American Ice Sheet Complex (NAICC) sprawled vastly over North America and had a profound impact on Earth's cryosphere (Hendy, 2009). The NAICC consisted of four different major ice sheets: the Cordilleran, the Greenland, the Innuitian, and the Laurentide ice sheets; each with their own special history and distinguishing characteristics (Figure 1.3) (Dalton et al., 2020).

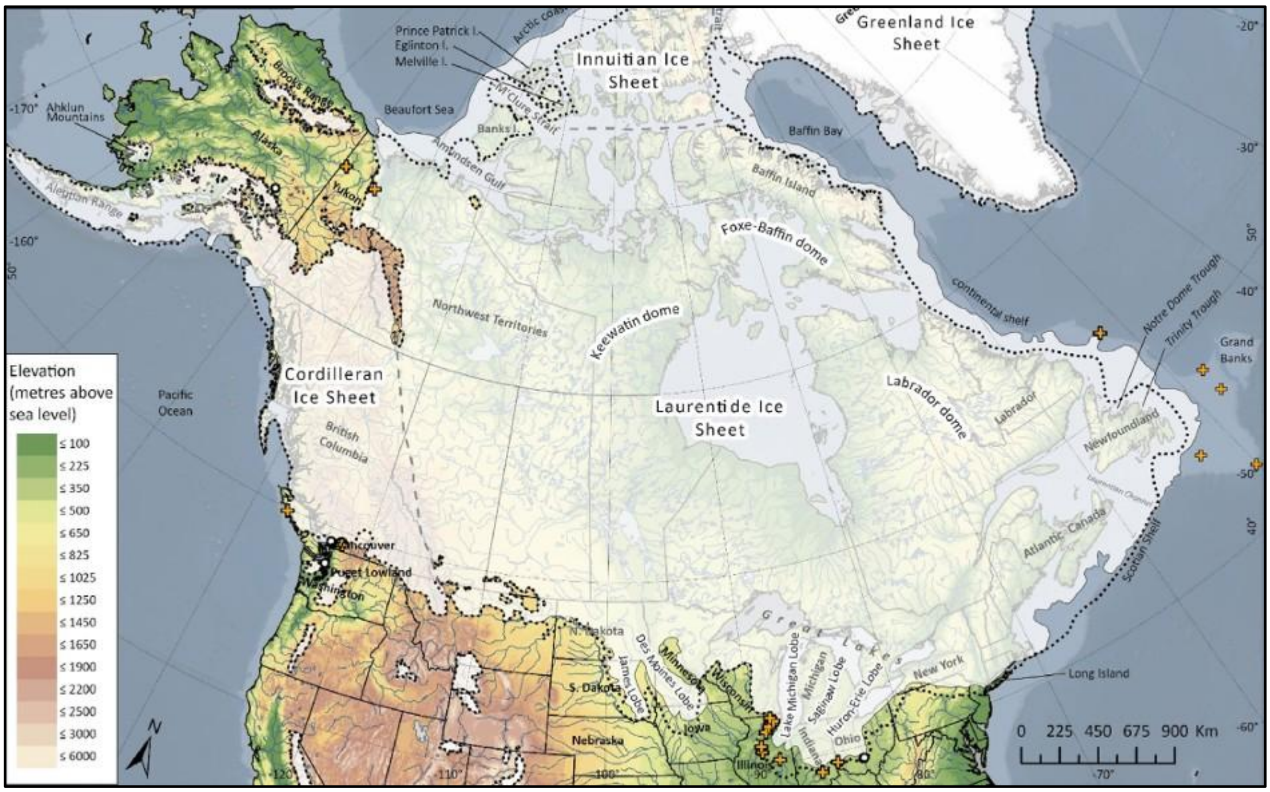


**Figure 1.3:** Figure depicting the Cordilleran, Laurentide, Innuitian, and Greenland ice sheets covering North America during the Last Glacial Maximum (LGM) (from Dalton et al., 2020).

The youngest and smallest of the ice sheets, the Cordilleran Ice Sheet (CIS), reached its maximum extent approximately 18,000 years ago (Dyke et al., 2004). The CIS advanced out of the mountains of Alaska and the Canadian Rockies approximately 25,000 years ago and spread southward covering an area approximately 4000 km wide at its maximum extent into the northwestern U.S. in line with the timing of the Fraser glaciation (Booth et al., 2004).

The Fraser glaciation was the last major glacial event that occurred in the Rocky Mountains of North America and is hypothesized to have occurred about 25 ka to 10 ka (Quirk et al., 2022). During the Fraser glaciation, the CIS extended south out of Alaska and Canada down into the continental U.S. forming various lobes of glaciers through the mountains and valleys of North America (Porter, 2004) (Figure 1.3). At their maximum extent, the CIS lobes covered an area of 4000 $km^2$ and extended as far west as the Juan de Fuca Lobe in Washington and as far south as the Puget, Okanogan, Columbia River, Purcell Trench, and Flathead Lobes in Washington, Idaho, and Montana (Hendy, 2009). It was the Flathead Lobe that extended off the CIS into its maximum position in the Flathead Valley sometime ca. 18.2 ka (Balbas et al., 2017; Hofmann et al., 2006) and dammed the Clark Fork River in northwestern Montana. This impoundment of the Clark Fork River resulted in hydrologic damming and backfilling of the landscape in northwestern Montana forming GLM (Figure 1.4) (Hendy, 2009).

At its maximum lake stand, it is hypothesized that the lake held a volume of 2600 $km^3$ and had a volume of 450 $km^3$ at its lowest level (Clarke et al., 1984; Smith, 2006).

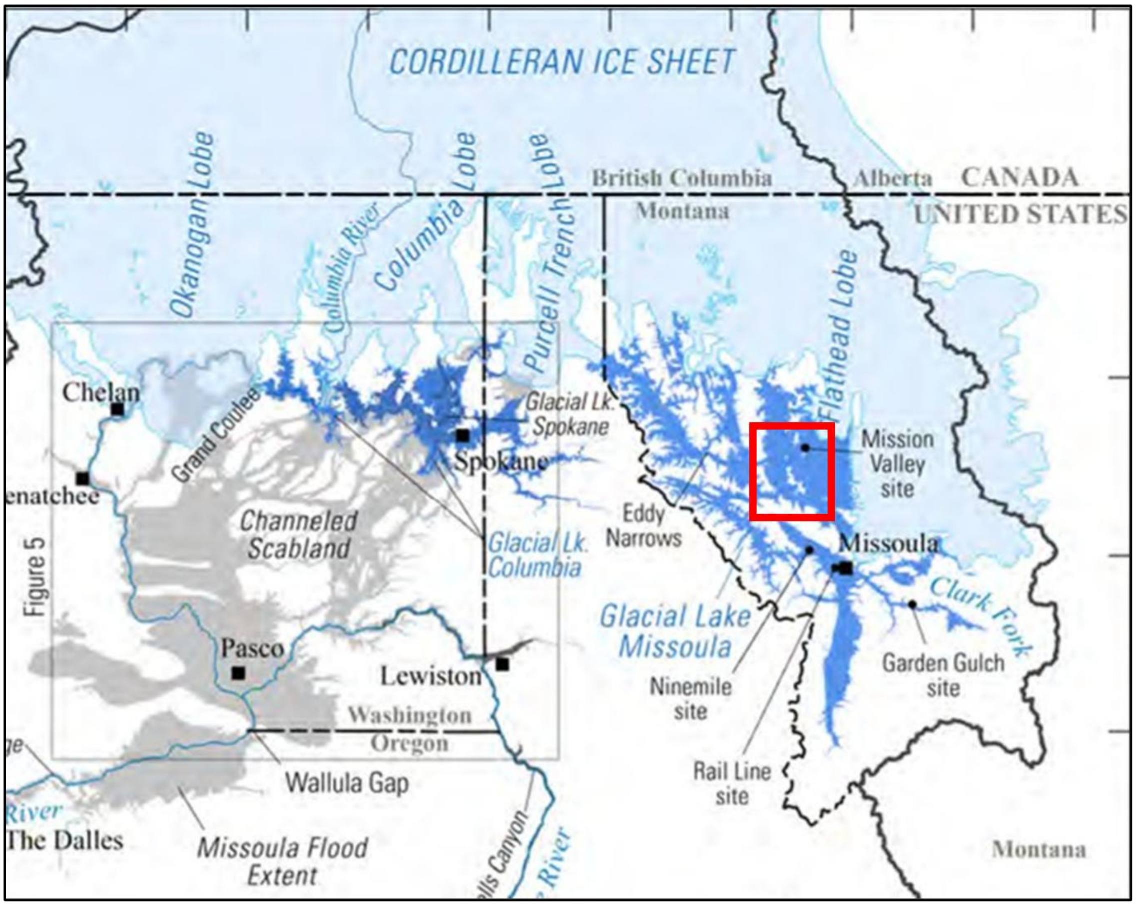


**Figure 1.4**: Mapped extent of the southerly reach of the Cordilleran Ice Sheet with the area of focus of this research highlighted in the red box in relation to the greater Channeled Scablands further to the west. Glacial Lake Missoula was formed from the damming of the Clark Fork River by the Purcell Trench Lobe off the Cordilleran Ice Sheet. The gray shaded area is the currently hypothesized mapped flood path of the Missoula floods. Modified from O'Connor et al. (2020).

Towards the end of its lifespan, repeated dam failures which are linked to the repeated thinning of the Purcell Trench Lobe based on sedimentological characteristics of catastrophic lake flood deposits that overlay glaciolacustrine deposits and $^{14}$C dating of tephra (O'Connor et al., 2020; Smith, 2006), caused catastrophic amounts of flood waters with discharge values exceeding 10-20 x $10^6$ $m^3/s$ (Alho et al., 2010) to drain through the Camas Prairie Basin leaving behind the Camas Prairie Ripples. While the path this flood took is relevant to this study, it should be known that there have been studies that have examined different flood paths across the Channeled Scablands in Idaho and eastern Washington (Figure 1.5) (O'Connor et al., 2020).

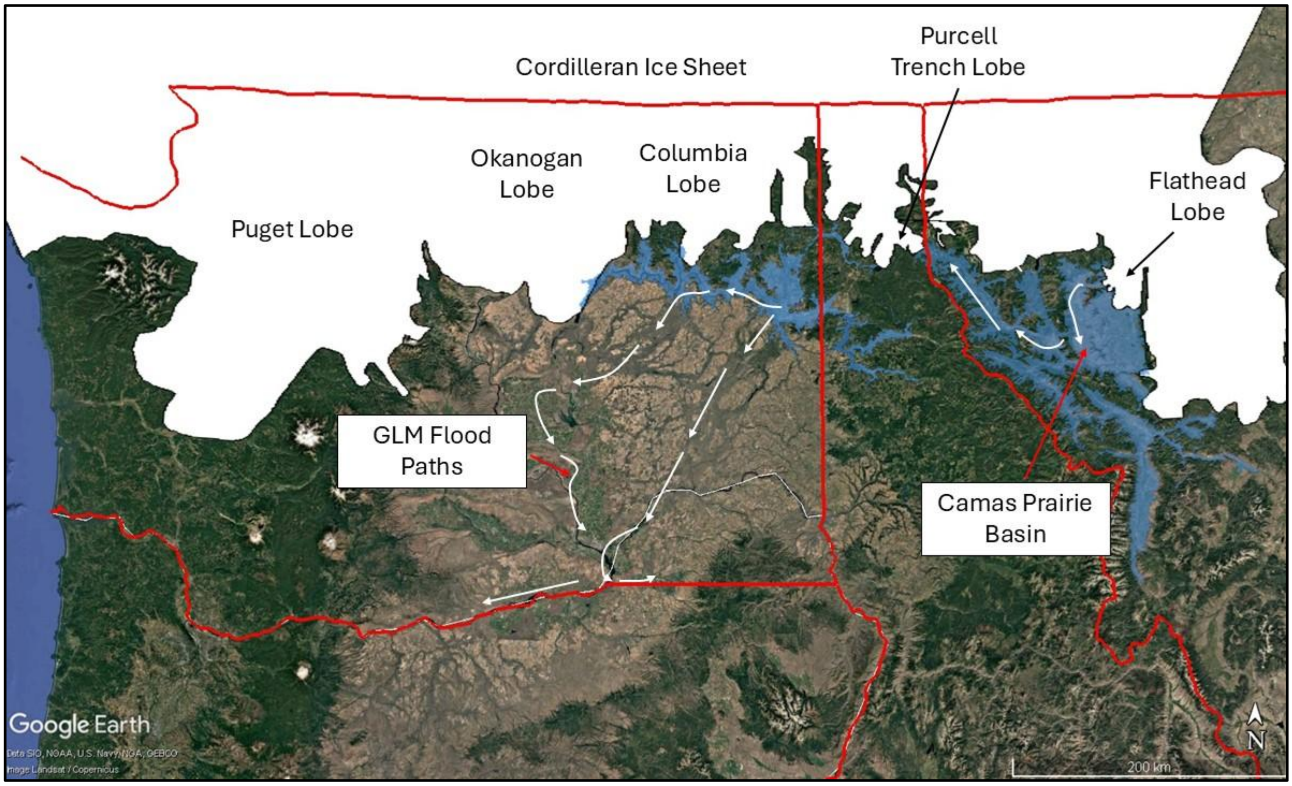


**Figure 1.5:** Google Earth™ image of the extent of the Cordilleran Ice Sheet with the lobes notated, and position of Glacial Lake Missoula and Glacial Lake Columbia shaded in blue. Flood path from Glacial Lake Missoula is denoted by white arrows. While the flood path in the Camas Prairie Basin is the most relevant to this study, it should be noted that there is evidence of different flood path for Glacial Lake Missoula and Glacial Lake Columbia in eastern Washington (O'Connor et al., 2020). Outline and shading for Glacial Lake Missoula and Glacial Lake Columbia courtesy of Ice Age Flood Institute and is available under Creative Commons license 2.0.

While the specific number of discrete flooding events is still disputed, it is generally thought that repeated dam failures occurred anywhere between 21.7 to 13.7 ka (Hendy, 2009; Smith, 2006; Smith et al., 2022).

Glacial lake outburst floods (sometimes referred to as GLOFs, jökulhlaups, or simply just outburst floods) are described as low-frequency, high-magnitude events with extreme hydrological characteristics (Figure 1.6) (Emmer et al., 2022). Outburst floods have been increasingly studied in the past two decades because of a need to understand occurrence trends, how they are linked to retreating glaciers globally, and their devastating impacts to communities worldwide (Harrison et al., 2018; Taylor et al., 2023). Evidence for these types of devastating floods is recorded in the dramatic geologic history of the Channeled Scablands and Columbia River Basin. It is estimated that a flood with a discharge of $17 \times 10^6$ $m^3/s$ in magnitude raced through Montana and eastern Washington on its way to the Pacific Ocean (Alho et al., 2010). However, stratigraphic and chronological evidence of glacial lake shorelines and lake sediments suggests that GLM emptied and refilled multiple times, indicating that there were potentially dozens of catastrophic floods (Alho et al., 2010; O'Connor et al., 2020; Smith, 2006). This debate, dubbed the "Great Scablands Debate" (O'Connor et al., 2020), is an area of active ongoing research to determine the timing and number of discrete flooding events that may have contributed to the flood features found in the Camas Prairie region and the Channeled Scablands.

**Figure 1.6:** Photo of flooding from glacial lake outburst flood that struck Juneau, Alaska back in August, 2024 taken by the United States National Guard. Creative commons license 2.0.

### 1.2.3 Previous Geochronology

Due to the complex and puzzling nature of these flood deposits, multiple studies have attempted to understand GLM chronology using a variety of Quaternary geochronological techniques. Identifying previous geochronologic data helps determine potential constraints on the likely age of flood features found in the Camas Prairie region.

Multiple studies have attributed the catastrophic flooding features found in the Channeled Scablands in eastern Washington and Idaho to GLM (e.g. Baker and Bunker, 1985; Benito and O'Connor, 2003; Hanson et al., 2012; Hanson and Clague, 2016). Baker and Bunker (1985) were among the first to constrain numerical ages to flood deposits in this region by examining deposits in the Channeled Scablands near Spokane, Washington by measuring the age of the Mt. St. Helen's S Tephra at a $^{14}C$ age of 16 and 12 ka BP. Benito and O'Connor (2003) then also examined this same tephra from Mt. St. Helens eruptions ("S" Tephra) that had been reworked and incorporated into flood deposits located in the Paco Basin in Idaho, and determined a radiocarbon age of 19-13 ka years $^{14}C$ BP, concordant with Baker and Bunker (1985). Pink, fine-grained sediment beds that are reminiscent of GLM lake-bottom sediments were found in Glacial Lake Columbia near Grand Coulee, Washington that had incorporated plant detritus which were measured to have a $^{14}C$ 13,400 ± 100 BP (Hanson and Clague, 2016). Another critical tephra that was used to, and is currently agreed to be the minimum age constrained to the Missoula floods, is the Glacier Peak tephra that was dated at 13.7 ka (O'Connor et al., 2020).

Attempts have also been made to understand sedimentological records of GLM floods and GLM's lake level fluctuations. Rhythmites that had been deposited near Ninemile, MT approximately 90 km to the south of the Camas Prairie Ripples and along the old rail line approximately 60 km south of Camas Prairie Ripples (Figure 1.4) were dated using OSL quartz techniques at 15.1 ± 0.6 ka and 14.8 ± 0.6 ka, respectively (Hanson et al., 2012).

Several sand-sized samples were collected at sand units directly above, below, and within glaciofluvial deposits in the Garden Gulch region of Montana, where there are records of lake-level fluxes like basal sand units, glaciolacustrine deposits, and bioturbated post-lake sediments (Smith et al., 2018). Based on OSL and infrared stimulated luminescence (IRSL) dating results from these sands, there may have been as many as potentially six cycles of lake level fluctuations over an approximately 2 ka timespan, and the bioturbated sediment that was deposited over the glaciolacustrine layer being directly dated at 10.6 ± 0.9 ka and at 11.9 ± 1.2 ka (Smith et al., 2018). It is important to note that these ages would have taken place after GLM floods, indicating potential inundation by GLM after flooding. Another study attempted to directly date some of the megaflood deposits located in Alberton Gorge located directly south of the Camas Prairie Basin by examining the luminescence signal at depth within gravels, termed rock surface luminescence. Out of 38 cobbles collected, Smith et al. (2022) measured the burial dose signal and calculated an average age of 17.5 ± 1.0 ka. This is similar to a cosmogenic nuclide age published by Balbas et al. (2017) by analyzing megaflood deposits in the Snake River section of the Channeled Scablands (18.2 ± 0.1 ka).

While most of these studies have not focused on the Camas Prairie Ripples, the data measured from samples in the Channeled Scablands helps to provide potential age constraints to the Camas Prairie Ripples found in northwestern Montana. If these features are sourced from the same floods that flowed through the Channeled Scablands, then the ages measured should fall somewhere in the range of radiocarbon and OSL data from the studies discussed above. Based on these studies from Smith et al. (2022), Smith et al. (2018), and the numerous radiocarbon and cosmogenic studies by Benito and O'Connor (2003), Hanson and Clague (2016), and Amidon and Clark (2015), we would expect to calculate a similar age for these features ranging from approximately 13.7 ka to 20 ka.

Despite all of the different data provided for potential flood ages in the Channeled Scablands, GLM lake-level fluxes, and flood deposits in northwestern Montana, there has not been any direct measurements to determine an age for the Camas Prairie Ripples, which are hypothesized to have been directly deposited from the outburst floods of GLM (Smith et al., 2022).

## 1.3 This Thesis

The aim of this study is to test and characterize quartz grains from samples collected from the crests of two giant current ripples and potentially determine a minimum age of deposition of the Camas Prairie Ripples, western Montana. Previous studies have linked sediment and floodwaters to GLM while attempting to constrain ages of GLM sediments using various radiocarbon and luminescence methods. Other studies have attempted to understand the complex history of Glacial Lake Missoula drainage using OSL and rock surface luminescence. Despite this, no chronologic data exists in the Camas Prairie. Camas Prairie Ripples are critical to understanding the paleohydrology of the drainage events of GLM (Alho et al., 2010; O'Connor et al., 2020; Smith et al., 2006) and understanding these processes can allow for more comprehensive understanding of other outburst floods.

Because of the catastrophic, highly energetic, turbid, and deep waters within which these ripples were deposited, the application of established OSL and other young Earth dating methods like cosmogenic nuclide dating to these sorts of deposits can prove challenging (Smith et al., 2022; Rhodes, 2011) as well as finding accessible localities to sample and excavate to collect for samples. For these reasons, little information is known about the exact timing of these features or whether they formed in a single, catastrophic event, or from repeated ice dam failures (Hanson et al., 2012; Smith, 2006). However, in similar challenging environments such as those dominated by fluvial and glaciogenic processes, combined luminescence and cosmogenic dating approaches can provide reliable and accurate ages (DeLong and Arnold, 2007; Spencer and Owen, 2004; Thrasher et al., 2019).

Given the challenge to using OSL in these types of environments (see Section 3.1.2), the objectives of this study are to use small aliquot OSL methods to determine the burial ages of sediments found in the Camas Prairie region. Partial resetting (bleaching) of prior luminescence in the quartz grains, which can lead to the overestimation of the burial dose (Fuchs and Owen, 2008), occurs in environments where light exposure is limited – like energetic, turbid waters hypothesized for the depositional environment of the Camas Prairie Ripples. Glacial and fluvial driven sediments may also have poor quartz luminescence characteristics if the bedrock from which the quartz originates is geologically young, if there are insufficient numbers of bleached grains, and insufficient dosing cycles prior to deposition (Spencer and Owen, 2004; Thrasher et al., 2009). However, there have been studies that have had success using established OSL techniques on quartz in these types of environments where there are poor bleaching conditions (Kalińska et al., 2025; Spencer and Owen, 2004; Spencer and Spencer, 2019).

This study attempts to use OSL techniques on quartz to test and characterize quartz grains from samples collected from the crests of two giant current ripples and potentially determine a minimum age sediment was deposited for the Camas Prairie Ripples. The hypothesis proposed is that if the Camas Prairie Ripples are the result of outburst floods from GLM, then the ages calculated should be comparable to reliable ages constrained to deposits published in existing literature in the Channeled Scablands and GLM. This involves the examination of geological evidence at stratigraphic depth within the ripple structure, including the overall sedimentology and geochronology of the features to determine a reliable age for the feature, and any stratigraphic layers that may be at depth within the ripple itself.

Appropriate sampling selections will allow for the measurement of ages for features in glacial environments. By comparing data measured in this study to other past geochronological and geologic studies, a better understanding of the depositional conditions of these features can be determined. Thus, putting their history in the context of the Quaternary history of GLM and the greater Channeled Scablands.

# Chapter 2 - Study Area and Sampling Sites

## 2.1 Study Area

GLOFs are cataclysmic floods that result from the release of high magnitude, low frequency flood waters from glacially dammed lakes (Emmer et al., 2022). These destructive floods often leave behind dramatic records in the stratigraphic record such as poorly sorted, angular, loosely cemented deposits like gravel bars (O'Connor et al., 2020). These types of features have been extensively studied to the east in the Channeled Scablands (Figure 1.5) with the main debate being how many flooding events may have caused these features. There are arguments for as many as 40 different floods (Waitt, 1980), a few flooding events (Smith, 2006), 100 different flooding events (O'Connor et al., 2020) or only one cataclysmic flood causing these features (Pardee, 1942). Now, studies have focused on examining the timing of potential flooding events from headwaters of GLM and its associated sublake notch systems (Figure 1.5).

GLM floods were hypothesized to have been channeled through four different sublake notch systems that directed different flows into the Camas Prairie Basin: Duck Pond Pass, Big Creek Pass, Markle Pass, and Wills Creek Pass Sublake Notch System (Lee, 2009). The Wills Creek Pass Sublake Notch System represents the largest of these systems based on the notch geometry and landform volume and extent volume (Lee, 2009; Bohorquez et al., 2019). This study focuses on ripples within the Wills Creek Pass Sublake Notch system (Lee, 2009) (Figures 2.1 and 2.2) because they are the most dramatic and appear to be the most anthropogenically undisturbed deposits compared to other ripple features found in the area (Lee, 2009). The Camas Prairie Ripples are labeled as Qg (Glacial, Fluvioglacial, and Flood Deposits) on a geologic map from Harrison et al. (1986) (Figure 1.2). They are described as torrential gravel deposits related to cataclysmic drainages from GLM, are sometimes located in perched valleys (e.g. Duck Pond

Pass), and can potentially show coarse cross-bedding in very limited exposures (Harrison et al., 1986). All samples for this study were collected in this geologic unit.

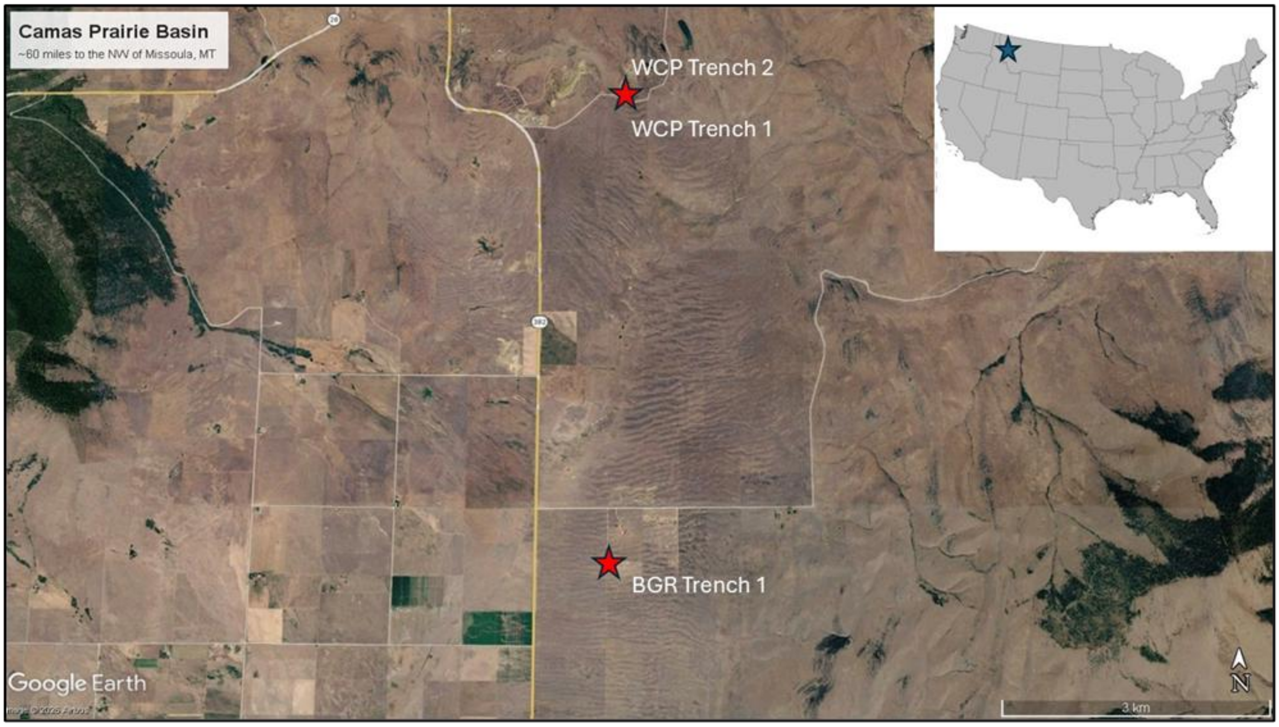


**Figure 2.1:** Google Earth$^{TM}$ image of the study area indicating sampling sites from both the Wills Creek Pass (WCP) and Big Gulch Road (BGR) trenches.

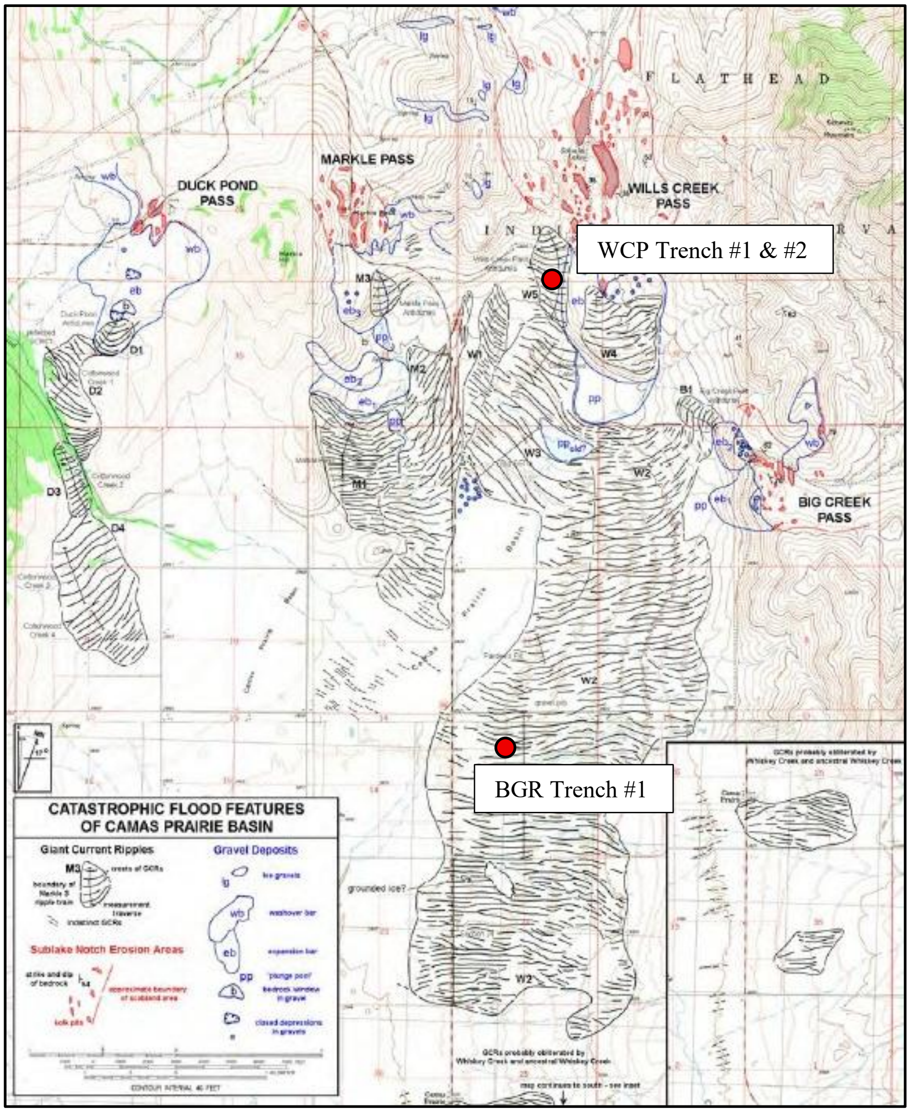


**Figure 2.2:** Map of the Camas Prairie located in northwestern Montana from Lee (2009). The two study areas (WCP and BGR) are noted by the red dots and are part of the overall Wills Creek Pass Subsystem noted by the hatched black areas.

## 2.2 Sampling Sites and Descriptions

Three separate trenches were opened using mini excavators (Figure 2.3) across the crests of three different ripples located at Wills Creek Pass (WCP) and Big Gulch Road (BGR) (Figure 2.2) in the Camas Prairie Basin. Two trenches were excavated near Wilks Gulch Road located in the northern part of the Camas Prairie Basin, and one trench was excavated at Big Gulch Road which is located in the south-central region of the Camas Prairie Basin (Figures 2.4 and 2.5).

**Figure 2.3**: Image of a trench being excavated located at WCP. Two trenches were excavated at this location. One trench being shown here (Trench #2) and one atop the crest of the ripple in the background (Trench #1). While no image of the excavator is shown, a trench was dug excavated at BGR using a similar Earth mover from a different landowner

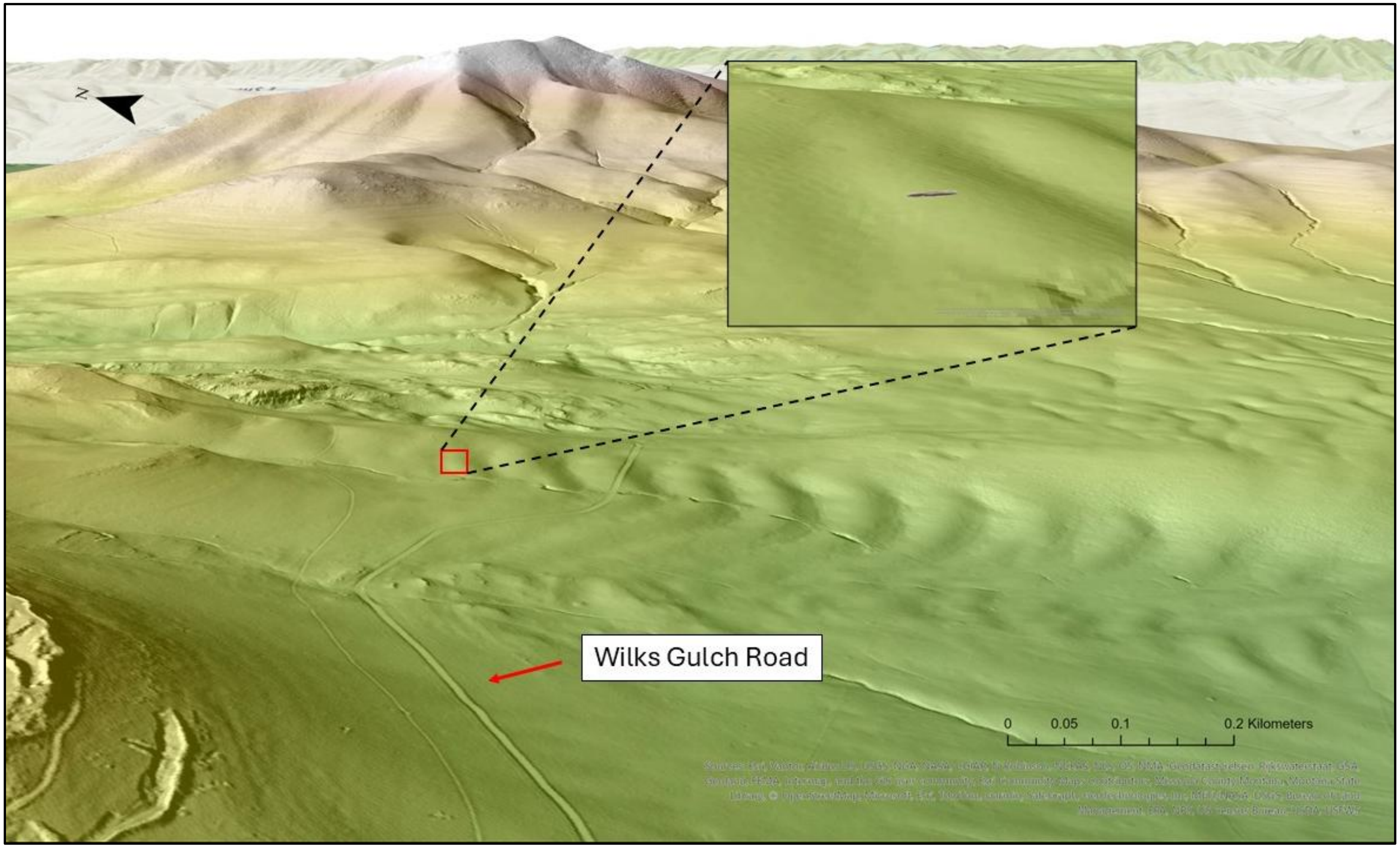


**Figure 2.4:** Image of trench excavated at Wills Creek Pass (see Figure 2.7 (A)) superimposed onto LiDAR data courtesy of the State of Montana. Trenches were excavated on or near the crests of the ripples.

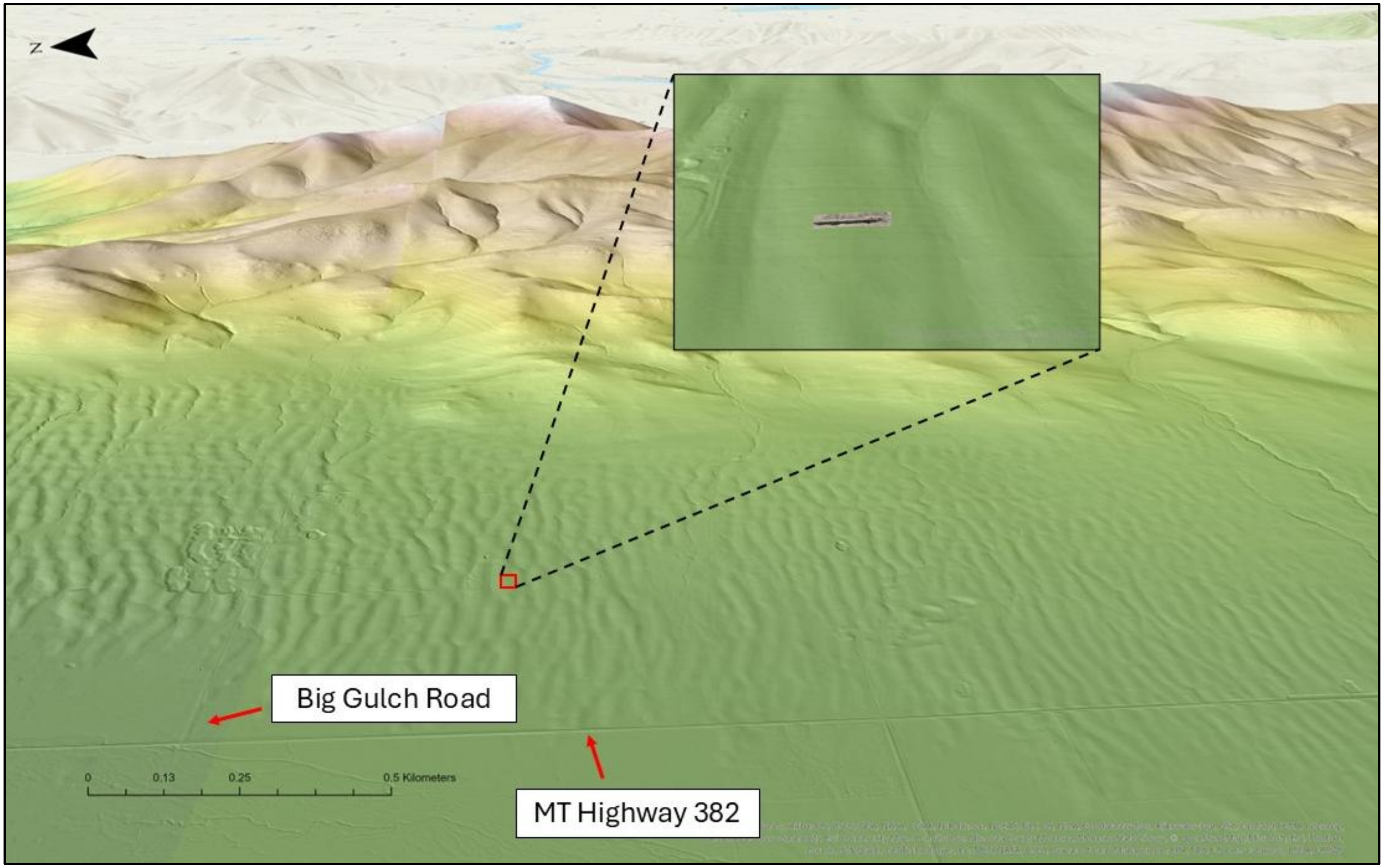


**Figure 2.5**: Image of trench excavated at Big Gulch Road (see Figure 2.7 (B)) superimposed onto LiDAR data courtesy of the State of Montana. Trenches were excavated on or near the crests of the ripple feature.

After trenches were excavated, trench walls were brushed with heavy duty brushes to clean up exposure facies and to remove any sediment that had been loosened by excavation. Multiple tarps were then used to cover each section of the trench as it was sampled, simulating dark conditions as much as possible (Figure 2.6) to prevent grains from being reset while collecting samples. As anticipated, since these features are large, poorly sorted, angular, loosely cemented deposits like those seen in gravel bars (O'Connor et al., 2020), typical sampling of sediment matrixes for OSL analyses using steel tubes was only possible in two localities in the BGR trench. For sediment matrix samples, the outer ~2 cm from the trench wall was removed so that any grains that were exposed during trench opening were not collected. Before sample collection, the horizontal and stratigraphic depth of each sampling locality was recorded to notate the sample's position in the trench. Matrix samples that were not collected in tubes were then collected in 5x8", 500 ml clear plastic bags while under the cover of darkness before being stored in opaque, black bags to protect grains from light while being transported to back Kansas State for laboratory analysis. Cobbles for future rock surface luminescence analyses were tagged with white spray paint (Figure 2.7), their vertical orientation marked with an arrow pointing to the surface, and horizontal and stratigraphic positions in the trench recorded. Cobbles were then extracted from the trench walls in similar dark conditions to the sediment matrix samples and wrapped in several layers of aluminum foil.

A total of 55 samples were collected from the three trenches in the Camas Prairie Basin. Fifteen sediment samples were taken from the two trenches located at WCP and seven sediment samples (two of these being traditional steel tube samples) from the single trench at BGR. Twenty-seven cobbles were extracted from the trenches located at WCP, while nine cobbles were removed from the trench located at BGR.

**Figure 2.6:** Image of the sampling setup located at WCP. It should be noted that a similar setup was used for all trenches. For each section of trench sampled from, samples were only collected from the darkest part that was covered by the tarp.


**Figure 2.7**: (A) Image of southern trench at WCP (Trench #2) excavated ~3 m wide and ~0.5 m deep. (B) Image of the trench opened at BGR ~5.5 m wide and ~0.5 m deep. Cobble samples were marked with white spray paint, had their “up” orientation relative to the surface notated, and then had their position horizontally and stratigraphically notated. Sediment samples had their positions notated in the trench and collected in black opaque bags to limit light exposure.

### 2.2.1 Wills Creek Pass (N 47°32.869’, W 114°35.440’)

Wills Creek Pass (WCP), located in the northern section of the Camas Prairie Basin, is part of the Wills Creek Pass Sublake Notch System (Figure 2.2) (Bohorquez et al., 2019). Two ~3 m long trenches were opened using a mini excavator (Figure 2.3). The sediments in these trenches were predominantly matrix-supported, cobble- to boulder- sized clasts ranging from ~7 to ~30 cm (Folk et al., 1970) (Figure 2.8). Prescence of matrix-supported sediment could indicate deposition under high energy type environments and mass-transport depositional processes (Blair and McPherson, 1999). Cobbles that were found in these trenches were overall much larger and more angular than clasts found at the BGR locality, potentially indicating cobbles here had been transported over less distance than those found at BGR. Samples were collected at increasing stratigraphic depth within the crest of the ripple to potentially reveal multiple flooding events through analyses and by examining potential depositional structures that are records of different flooding events following Kalińska et al. (2025).

**Figure 2.8:** Photo of a section of the trench excavated at Wills Creek Pass showing larger and more angular clasts compared to the matrix found at Big Gulch Road.

### 2.2.2 Big Gulch Road (N 47°29.670', W 114°35.684')

Big Gulch Road (BGR) is located approximately 6 km to the south of the WCP locality in the Camas Prairie Basin and is still located in the Wills Creek Pass Sublake Notch System (Bohorquez et al., 2019). One ~6 m long trench was excavated at the crest of a ripple (Figure 2.9). The clasts found at this location are much smaller than those at seen at WCP (Figure 2.10) ranging from ~7 cm to 17 cm which would be classified as pebbles and cobbles following the classification scheme used by Folk et al. (1970). Conversely, the sedimentary framework of the trench at BGR would be classified as clast supported, potentially indicating lower depositional flow velocities than those found at WCP (Blair and McPherson, 1999). However, compared to WCP, clasts found here were more rounded compared to those found in the WCP locality, potentially meaning that energy conditions lessened father away from the notch system and larger clasts had been dropped out of the flow regime as they spilled out into the basin (Carling, 1999). The presence of rounded clasts could also indicate that these clasts had been carried for longer in the transport system than those found at the WCP locality. As opposed to the trenches at WCP, no potentially identifiable structures were identified in this locality. Similar to WCP, sediment matrix and cobbles for future work were taken at depth stratigraphically to potentially constrain multiple flooding events.

**Figure 2.9:** Image of the trench excavated at BGR. The trench was approximately one-meter deep and approximately six meters wide.

**Figure 2.10:** Image of matrix from the BGR trench. Clasts are much smaller compared to those found the WCP locality. The clasts found here are much rounder compared to the angular clasts found at WCP. The fabric found at this locality is mainly clast supported, indicating a higher flow velocity at this locality.

# Chapter 3 - Methods and Results

## 3.1.1 OSL as a Dating Technique

Optically stimulated luminescence (OSL) dating is a young Earth dating technique that is used to determine when mineral grains were last exposed to daylight within the past 200,000 years (Rhodes, 2011). In quartz and feldspar grains, electrons and holes (referred to as charge), are stored within defects in the crystal lattice that form from radiation in the surrounding environment and minerals (Rhodes, 2011). The last daylight exposure removes any prior stored charge – resetting the dating clock. Upon deposition and burial, trapped charge accumulates again due to radiation exposure from the surrounding environment and minerals over time that can then be liberated in the lab optically to determine the natural dose. The natural luminescence signal is then compared to the luminescence signal generated by subsequent laboratory radiation put into the grains to calculate the amount of radiation that accumulated in the grain since deposition (Mahan et al., 2023). The single-aliquot regenerative-dose (SAR) protocol of Murray and Wintle (2000, 2003) is an accurate and reliable protocol that is applied to OSL measurements (shown in Table 3.1) (Rhodes, 2011) to determine the equivalent dose. At each sampling locality, the environmental dose rate that the grains are subjected to is also measured and calculated to be used to determine the age of sediment deposition (Rhodes, 2011).

Constraining ages to features using OSL is a function of dividing the equivalent dose by the environmental dose rate:

$$age = \frac{equivalent\ dose\ (D_{\mathrm{e}})}{environmental\ dose\ rate\ (D_{\mathrm{r}})}\ \text{, [ka = Gy/(Gy/ka)]}$$

Where the equivalent dose ($D_e$, measured in grays (Gy)) is the amount of radiation energy trapped in the grain since the OSL traps were last emptied. The environmental dose rate ($D_r$) is the rate at which the dose is deposited by ionizing radiation from radioactivity from the mineral grains and the burial environment (Mahan et al., 2023).

In luminescence dating, light sensitive traps in quartz grains are stimulated using blue and green LEDs or lasers, and the emitted luminescence detected in the ultraviolet (UV). Although luminescence from feldspar grains can also be stimulated with blue-green light and detected in the UV, they are most efficiently measured using near-infrared LEDs or lasers with light emission detected in a broad blue-violet waveband (Wintle and Murray, 2006). Similar to feldspars, the emission spectra of quartz typically varies, and can be strongly influenced by presence of impurities and type of excitation used (Krbetschek et al., 1997). While quartz grains typically emit ultraviolet (UV) light, it has also been shown they can emit other visible and near-infrared wavelength bands (Krbetschek et al., 1997). For quartz OSL, UV detection filters are used with blue/green stimulation to limit the amount of stimulation light reaching the PMT, thus reducing the measurement background of the instrumental setup. The emitted light emissions are then counted to estimate the equivalent dose (Wintle and Murray, 2006). $D_e$ calculations are completed by using the SAR protocol (Wintle and Murray, 2006; Murray and Wintle, 2003).

### 3.1.2 Challenges to OSL in Proximal Glacial Environments and Outburst Flood Deposits

One of the core aspects and assumptions used in OSL dating is that the traps were completely or nearly empty at the time when the sediment was buried (referred to as being "bleached"). One crucial factor controlling if a grain has been bleached is the depositional environment in which the sand grain was deposited. Certain depositional environments allow for better bleaching of grains than others (Figure 3.1) (Rhodes, 2011). Glacial environments can present challenges to using established OSL techniques.

One factor that can present challenges to using established OSL techniques is proximity to the ice margin since shorter transport times can lead to less time for adequate bleaching. Debris, or ice-covered surfaces, typically seen in glaciofluvial or fluvioglacial transport can present challenges to established OSL techniques since this can hinder any daylight resetting of grains. Poor quartz characteristics (i.e., poor luminescence sensitivity or dim light levels) are often found in glacial and proximal glacial settings (Rhodes, 2011). Additionally, these types of environments typically had more cloudy days in snow/ice settings, decreasing the likelihood of homogenous bleaching (Zhu et al., 2022). Taking all of this into account, the mechanisms (i.e., glacial, catastrophic flood, or both) that the sediment were subjected to are unknown and could have likely lead to incomplete bleaching.

Incomplete bleaching coupled with analysis of multi-grain aliquots is a critical issue in luminescence dating. A multi-grain aliquot is when a sample is composed of multiple grains and is used to determine the burial age of the sediment through luminescence dating methods. Complete bleaching of grains is particularly important. If the grains in the sample have not been fully bleached, the equivalent dose, and therefore OSL age calculated, will include residual doses from prior radiation exposure leading to an overestimation in age when combined with the burial dose (Galbraith et al., 1999). Given the catastrophic, highly energetic, turbid, and deep waters within which these megaripples were deposited (Lee, 2009; Alho et al., 2010), the likelihood of daylight bleaching of sufficient number of grains to derive accurate depositional ages with luminescence approaches is small (Thrasher et al., 2009).

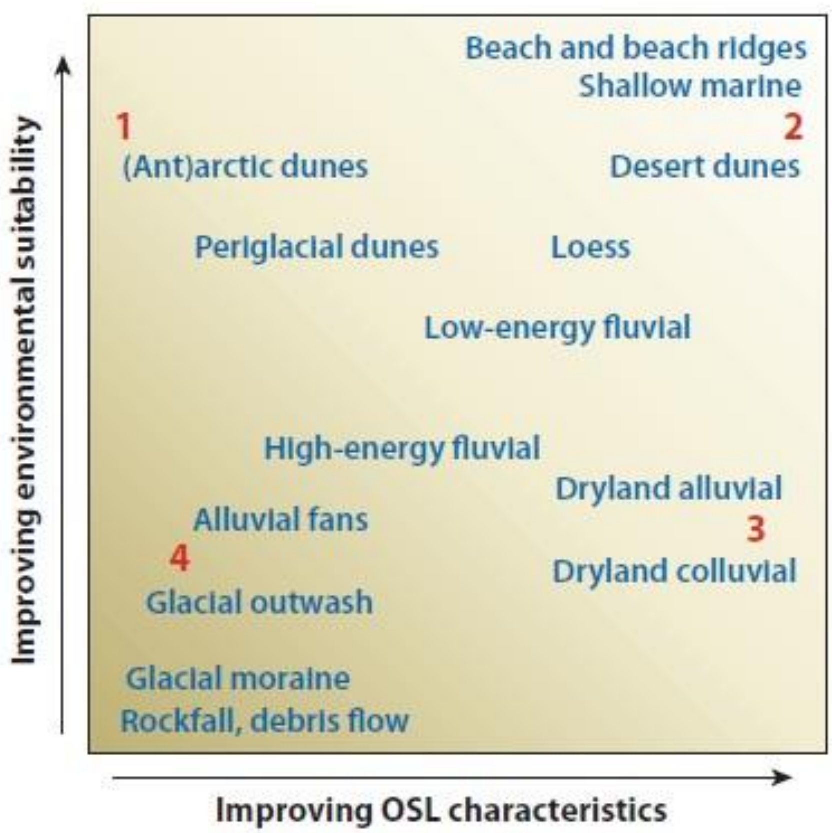


**Figure 3.1:** The degree of bleaching for environments is going to vary based on depositional energy, amount of daylight exposure, and mechanism of sediment transport. Grains that are deposited in environments where daylight is near constant will bleach grains adequately like beach and desert environments, where high energy depositional environments like glacial environments will bleach poorly. From Rhodes (2011).

However, previous studies have examined the potential of using OSL in glacial environments and have even found some successes (Spencer and Owen, 2004; Thrasher et al., 2009). Spencer and Owen (2004) found that quartz signals bleach in daylight easier than feldspar grains, and their quartz data were consistent with the chronologic framework from cosmogenic nuclides at the study site. Another OSL method that has gained relevance in dating glacial deposits is rock surface luminescence. Rock surface luminescence (introduced in Section 1.2.3) allows for the analysis of clasts that have undergone complex bleaching or incomplete bleaching histories (Smith et al., 2022). Despite there being challenges to luminescence dating of features in glacial environments, some studies have had success constraining ages to these types of features using a combination of established OSL techniques (i.e., small aliquot analysis on quartz and feldspars), rock surface luminescence, and $^{10}Be/^{26}Al$ cosmogenic nuclide dating (DeLong and Arnold, 2007; Fuchs and Owen, 2008; Thrasher et al., 2019). Based on promising initial data measured on quartz from the tube samples collected at the BGR locality (see further discussion in Section 3.2.3 below), small aliquots of quartz were analyzed in this study for the remaining samples from the sediment matrices.

## 3.2 OSL Methods and Results

### 3.2.1 Sample Collection and Preparation

Samples were collected from the Camas Prairie Basin (Figure 2.1). Two different sampling sites were chosen. One was located in the northern section of the Camas Prairie Basin and the other was located in the central part of the Camas Prairie Basin (Figure 2.2). Trenches were excavated at the crests of three ripples; the first two at WCP and the third at BGR (Figure 2.2).

**Figure 3.2:** Photo taken of an excavated trench located at Wills Creek Pass. Matrix samples had their orientation along the trench notated and excavated. Cobble samples were marked with white spray paint, had their upward facing orientation denoted and had trench position recorded.

A total of 55 samples were collected from the three trenches. Twenty-one matrix samples were collected for luminescence analysis, and 34 cobbles were collected for future rock surface luminescence and cosmogenic nuclide analysis. Of these, 15 matrix and 27 cobble samples were collected from the WCP trenches and seven matrix, and nine cobble samples were sampled from a trench at BGR. Samples were collected following protocols listed in Section 2.2.

Preparation of sediment matrices was carried out as follows:

[1] Samples were prepared under low-intensity amber LEDs. This combination of amber LEDs and low-intensity light was used to prevent any luminescence signals from being erased

during preparation. It should be noted though, while this combination is specific to minimize signal loss in feldspar grains, quartz grains can also be prepared under these conditions.

[2] Approximately half the sample was set aside for ICP-MS/-AES analysis to determine the environmental dose rate so that a representative portion of the sample was analyzed for ICP-MS/-AES since different grain sizes can take in radiation of different rates than others (Softa et al., 2021). These half portions were weighed before being dried overnight at 50°C in the oven. The next day, the samples were weighed again until the weight of the sample was stable to examine and determine field moisture in the sample; important since water attenuates the alpha, beta, and gamma radiation that interacts with the sample (Durcan et al., 2015). Using a 2 mm sieve the dried sediment was separated into <2 mm and >2 mm fractions for individual ICP-MS/-AES analysis; mass of the <2 and >2 mm fractions was recorded. Approximately 20 ml of each sieve fraction of sediment from each sample was pulverized using a Shatterbox® with a tungsten carbide ring and puck mill. Approximately, 10 g of this sediment was then analyzed at SGS Canada Inc. in Burnaby, BC, Canada using ICP-MS/-AES to determine the elemental concentrations of K, Th, U and Rb.

[3] For the part of sample used for $D_e$ analyses, ~100 g of sediment was first wet sieved using 63 µm, 90 µm, 125 µm, 180 µm, 212 µm, 250 µm mesh sieve fractions and then left to air dry overnight. Once dry, the sieve fractions were then dry sieved. The grain size chosen for analysis was the modal grain size of the distribution between 250 µm and 63 µm (for all samples in this study this was the 125-180 µm fraction). [4] The grains of the chosen grain size were then treated using 10% hydrochloric acid (HCl) for ~30 minutes to dissolve adhering carbonates and 30% hydrogen peroxide ($H_2O_2$) for ~3 days to remove any organic matter. Samples were then washed in deionized (DI) water to remove any $H_2O_2$ and material in suspension, washed in

acetone to remove any leftover water, and dried in the oven briefly at 50°C until grains were dry and free flowing.

[5] After chemical treatment, samples were then floated using lithium metatungstate (LMT) solutions with densities of 2.70 g/cm$^3$ and 2.58 g/cm$^3$ to separate quartz-rich (2.70-2.58; principally quartz, plagioclase, and Na-feldspars) and K-rich feldspar (<2.58) grains. [6] After being floated through both LMT solutions, the quartz and feldspar fractions were then washed in DI water and acetone and dried briefly at 50°C. Quartz fractions were then treated with 48% hydrofluoric acid (HF) for 40 minutes to dissolve any remaining feldspar minerals leftover. Also, the HF treatment step is used to remove an ~10-20 µm rind which minimizes the luminescence signal from alpha particles external to the grain. HF treatment can have the added benefit of removing adhering crusts such as iron oxides and may help "clean" the grain surface improving light transmission into and out of the grains but equally can cause frosting and pitting of grain surfaces. Afterwards, samples were then washed in 10% HCl to dissolve any fluorides precipitated. Then the washing and drying steps from above were repeated one more time. After this, the grains were then dry sieved one more time using a 90 µm sieve mesh to remove any smaller grains or particles that remain after HF and HCl dissolution.

Multi-grain aliquots of quartz 1-mm in diameter were mounted in the center of ~10 mm stainless steel discs using Silkospray™ silicone spray and spray templates. The number of grains mounted on a 1-mm aliquot is approximately 30-50 grains for the 125-180 µm size sieve fraction. The prepared K-rich feldspars were retained in the laboratory archive for future analysis in follow-on projects.

### 3.2.2 Feldspar Contamination

Sediments in this locality contain a mixture of both quartz and feldspar minerals. The differing luminescence properties of quartz and feldspars (e.g., slow and fast components) can affect equivalent dose measurements (Figure 3.3) (Thomsen et al., 2008). In quartz analysis, removal of feldspar minerals is important since K-rich feldspars are typically significantly brighter, and feldspar grains emit luminescence when stimulated by the same blue-green light sources typically employed to stimulate quartz. So, it is critical to either ensure adequate separation of minerals or, failing this, optically remove the feldspar signal before quartz measurement. Typically, quartz and feldspar minerals are separated using both physical means (i.e., liquid density separation) and chemical means (dissolution of feldspars in HF) (Wintle, 1997). In the case of these sediment samples, it was determined that samples contained significant feldspar grains based on their high counts when measuring IR signals (Figure 3.3). Therefore, extra steps in the treatment process were required to clean up the OSL signal and remove any feldspar contamination.

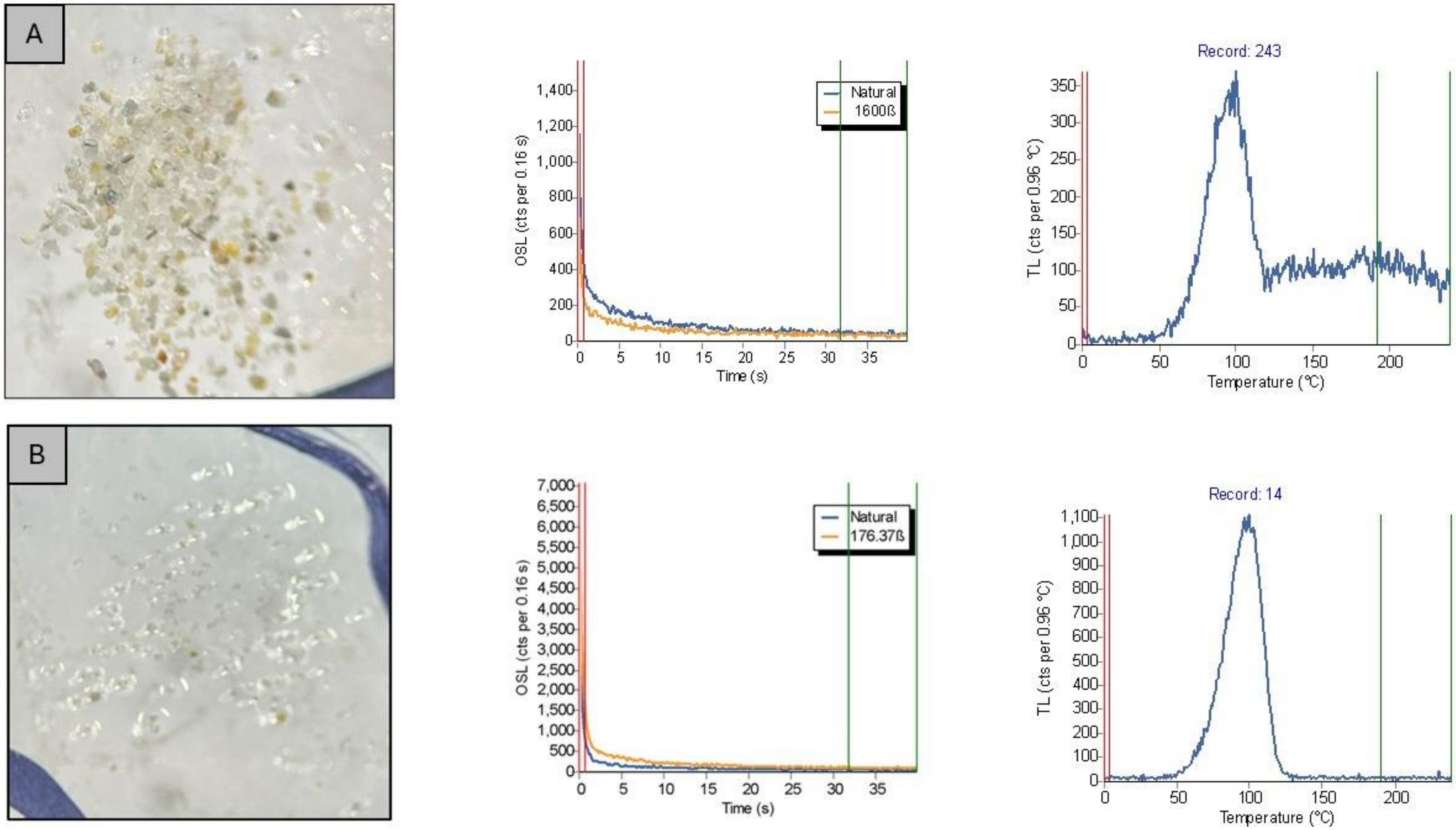


**Figure 3.3:** Comparison of samples before (A) and after (B) magnetic separation. (A) Feldspars typically emit more of the slow component of the OSL decay curve causing a broader curve. When examined under a binocular microscope, feldspars appear opaque. Feldspars are both stimulated and measured using blue-OSL measurements, which weaken their signal. (B) Quartz's OSL decay curve will typically have more of the fast component, and quartz minerals will appear glassy and see-through under a microscope. Discs contaminated with feldspars and other minerals will show a shoulder at 110°C during TL measurements, making TL measurements a powerful tool in identifying contamination on a disc.

One of the more uncommon methods taken to physically clean up the mineral grains uses magnetic separation to separate the feldspar grains from quartz grains (Aitken, 1985; Rosenblum, 1958). By using a Frantz LB1 with a high current on the magnet, sediment samples that contained feldspars were able to be cleaned up, leaving mostly quartz grains behind since quartz and feldspar can be separated due to having differing magnetic properties (Porat, 2006). Effective separation was determined by observing a small sample of non-magnetic fraction under a binocular microscope and observing that there are little to no dark or opaque minerals present, essentially indicating that there are only mostly quartz grains present (Porat, 2006). Depending on the material that is being separated, the settings for the Frantz magnetic separator may need to be changed slightly. However, in general, the optimal settings for these samples were found to be:

Slope of 25°, tilt of 17°

Volts: 100.3 - 101.4

Current: 1.51 Amps on the magnet

Additionally, extra time in HF can also be employed to remove any contaminant minerals left in the sample after magnetic separation (Porat, 2006). Afterwards, grains were then loaded into the instrumentation (see following Section 3.2.3) for luminescence measurements.

Furthermore, certain luminescence measurements can be used to minimize feldspar contamination in a given aliquot. As discussed more in Section 3.2.3., a post-IR blue measurement can be made to optically bleach with infrared stimulated luminescence (IRSL) the signal of any remaining feldspar grains left in an aliquot (Şahiner et al., 2014), leaving just the quartz OSL signal. In addition to analyzing for any remaining contaminant signals, this step can also be used to reduce the signal of any feldspar grains, since they will often appear brighter than regular quartz grains (Thomsen et al., 2008).

### 3.2.3 OSL Measurements and $D_e$ Assessment

All multi-grain luminescence measurements were measured at Kansas State University's Luminescence Dating Lab using a Risø TL/OSL reader model DA-20 (Bøtter-Jensen et al., 2003) equipped with a $^{90}Sr/^{90}Y$ beta source with a dose rate of ~ 0.118 Gy/s. Blue LEDs (470 nm) were used for quartz stimulation and infrared LEDs (870 nm) were used for stimulation of feldspar minerals. All signals were detected in the UV using 7.5 mm of Hoya U-340 filter and an EMI 9235QB photomultiplier tube (PMT).

The measurement sequence and SAR protocol are outlined in Table 3.1. The SAR protocol is composed of six steps. Step 1 involves administering the regenerative dose, or no dose if measuring the natural dose. Step 2 involves pre-heating the sample for 10s at 260°C to remove unstable charge from shallower traps before measuring the stable signal. Pre-heat temperatures were determined by SAR protocols passing dose recovery tests (See Section 3.2.5). Step 3 measures the samples using IR stimulation to optically bleach the signal from any contaminant feldspar grains on the disc (Şahiner et al., 2014; Thomsen et al., 2008). Step 4 measures the quartz luminescence signal using blue light stimulation. This is where the natural or regenerative OSL signal was measured (Lx). Step 5 is administering a test dose which is usually 15-25% that of the average De (Figure 3.4). However, since the quartz measured was insensitive (see Section 3.2.7), a higher test dose was used in some cases. A cut heat is implemented in step 6, which is typically 20°C less than the pre-heat step. This is to test any thermal transfer from quartz, test for any feldspar contamination in subsequent measurements, remove any shallow unstable traps, and remove any possible ultra-fast component of the quartz OSL signal (Figure 3.4) (Murray and Wintle, 2003; Tsakalos et al., 2020). Step 7 is another IR measurement to separate differing signals of quartz and feldspar and to assess any feldspar contamination in a similar vein to Step 3. Finally, Step 8 is a final OSL blue measurement to analyze the test dose luminescence signal (Tx) compared to the natural or regenerative OSL measurement in Step 4.

**Table 3.1:** SAR sequence based on Wintle and Murray (2006). Data to enable equivalent dose ($D_e$) calculation were measured in Steps 4 and 8.

| Step | Treatment | Observation |
|---|---|---|
| 1 | Give regenerative dose | |
| 2 | Pre-heat: 260°C for 10s (varies per sample) | |
| 3 | IR LED stimulation: 40s at 50°C | |
| 4 | Blue LED stimulation: 40s at 125°C | Lx (natural or regenerative OSL dose |
| 5 | Test Dose: 100-400s | |
| 6 | 240°C cut heat test | |
| 7 | IR LED stimulation: 40s at 50°C | |
| 8 | Blue LED stimulation: 40s at 125°C | Tx (OSL response to small test dose) |
| 9 | Return to Step 1 for Run 2 | |

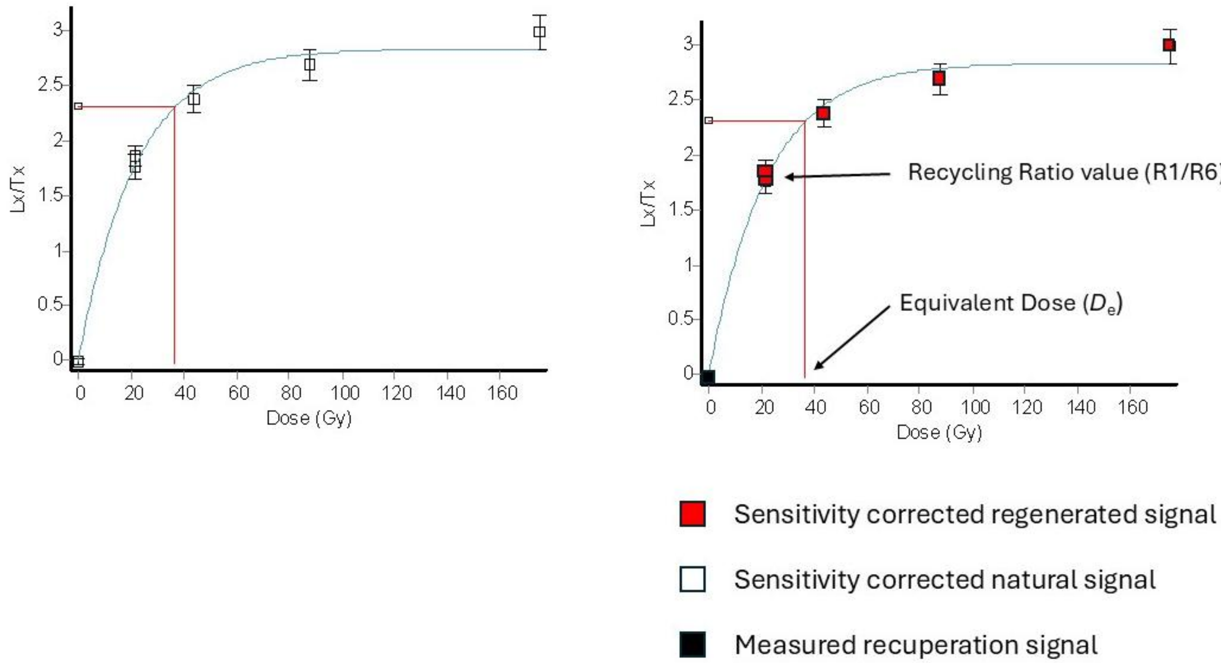


**Figure 3.4:** A typical growth curve from one of the aliquots from the 25WCP-08 sample. For each aliquot, the sensitivity-corrected natural signal, $L_n/T_n$ (white square) is interpolated with the line of best fit that is fitted using a single saturating exponential function by fitting the regression through sensitivity-corrected regeneration dose points, $L_x/T_x$ (red squares).

Due to the limited amount of material collected at each trench, initial measurements were conducted on tube samples collected at BGR, since those samples followed more established OSL sampling procedures (Mahan et al., 2023). Initial tests of the tube samples (25BGR-15 & 25BGR-16) collected at BGR showed good behavioral characteristics for quartz luminescence as indicated by showing a dominant fast component in the quartz as well as acceptable recycling ratio (1.01 ± 0.04 %) and recuperation values (1.2 ± 0.2%), and initial $D_e$ data consistent with perceived age range based on typical quartz dose-rates of ~1-2 Gy/ka. Based on these initial values, it was thought that luminescence minerals on quartz would yield acceptable data, so the rest of this study focused on further examination of the quartz data.

### 3.2.4 Recycling Ratio Test

The recycling ratio test is a characteristic test in the OSL dating process that determines how reliable OSL measurements were made by assessing if the SAR protocol is able to correct for any changes in sensitivity (Wintle and Murray, 2006). The recycling ratio is simply the ratio of two laboratory and test dose measurements (Lx/Tx) of the same regenerative dose and is typically the first and last regenerative dose points of the SAR cycle that are repeated. Ideally, these values should be the same, giving a recycling ratio of 1, but ratios between 0.9 and 1.1 are considered acceptable (Murray and Wintle, 2003, Wintle and Murray, 2006). For example, the recycling ratio of 25WCP-21 has an average recycling ratio of 1.06 ± 0.13 over 18 accepted aliquots which are within acceptable limit. Once the recycling ratio is complete, OSL measurements can be continued (Murray and Wintle, 2006).

### 3.2.5 Dose Recovery Test

The dose recovery test is an assessment of the effectiveness of the SAR protocol in OSL dating. The main aim of the test is to determine if the SAR protocol can accurately measure a known dose of radiation after bleaching, and if it can measure a dose that is recovered from the sample (Murray and Wintle, 2003). Passing this tests ensures that SAR protocol is able to accurately measure the equivalent dose in the sample (Wintle and Murray, 2006). To test this, two aliquots from each site (WCP Trench #1 and BGR) had their signal bleached optically, had a 1000 s regenerative dose administered, and then had the SAR protocol outlined in Table 3.1 tested on it. The results are given in Table 3.2. As discussed in the next section below, many of the grains in the aliquots analyzed in these samples were saturated, making it difficult to measure the dose of the grains after irradiation. Some of the aliquots analyzed in the samples for dose recovery tests were approaching saturation (see Section 3.2.6). So, to identify their measured dose value and associated error, the ratio of Ln/Tn to Lx/Tx was used, where Lx/Tx is the regeneration data from a 1000 s dose. These ratios were used to calculate the measured signal and error for the dose recovery test.

**Table 3.2:** Dose recovery test for each of the three localities. The given dose is similar to the average De measured for each sample. Results are the average measured/given (M/G) ratios for of all aliquots of sample at each locality.

| Sample Name | Given (s) | Measured (s) | M/G |
|---|---|---|---|
| 25WCP-19 | 1000 s | 904.50 ± 100 | 0.90 ± 0.10 |
| 25BGR-06 | 1000 s | 905 ± 90 | 0.91 ± 0.09 |

### 3.2.6 Dose Saturation

In OSL dating, the upper limit of the age range is primarily controlled by dose saturation, which is where all of the OSL traps have become filled resulting in no more charge becoming trapped within defects in the crystal lattice (Rhodes, 2011). Different minerals will typically saturate at different doses. It has been shown that, typically, quartz saturates at much lower doses compared to feldspars (Faershtein et al., 2019; Rhodes, 2011). This limits the maximum age limit for quartz OSL dating to approximately 200,000 years. A typical OSL growth curve that shows saturation is shown in Figure 3.5. Interestingly, in many of the samples collected from the CPR, the measured aliquots saturate early around the 80 Gy mark compared to the typical saturating point at ~100-200 Gy. This 80 Gy mark was determined by examining where on the dose response curve saturation begins (Figure 3.5). Despite this, because of the limited number of aliquots that were accepted, it was found that more aliquots were needed to be analyzed from the samples in order to get enough data to be tested using various statistical models. If aliquots that display saturation are run through statistical models though, it should be noted that this can result in an underestimation of ages by causing a skew in data towards the lower set of data (Chapot et al., 2022; Faershtein et al., 2019).

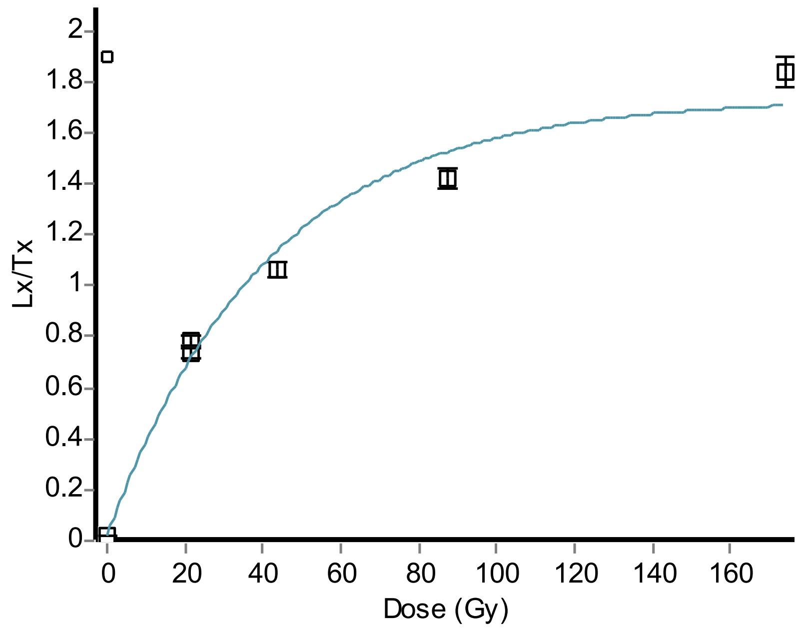


**Figure 3.5:** Dose response curve from 25BGR-06 sample that shows quartz grains saturating early. From this, $D_e$ values cannot be measured since values cannot be interpolated on the x-axis because the dose response curve flattens. The aliquot is saturating at the 80 Gy mark where the dose response curve starts to plateau. Aliquots that demonstrate saturation can be evaluated using criteria described by Spencer and Robinson (2008) and removed from the analysis.

### 3.2.7 Test Dose Examination

The test dose in the SAR protocol exists to monitor any sensitivity change during $D_e$ measurement using the SAR protocol. When examining the luminescence signal in the lab, heating and optically stimulating the grain can alter how charge is transferred in the mineral grain, causing the grain to emit more or less light per unit dose (Murray and Wintle, 2003). Essentially, the test dose is given to determine whether the luminescence per unit dose changes in each regenerative SAR cycle and, if so, correct the preceding regenerative luminescence for increase or decrease in sensitivity – hence Lx/Tx terminology in Table 3.1 and Figures 3.4 and 3.6. When there is insensitive quartz, it limits the number of $D_e$ values that can be determined (Mahan et al., 2023). In more routine measurements, it is typically recommended that the test dose value is 15-25% of the average $D_e$ values (Murray and Wintle, 2003; Mahan et al., 2023).

In initial measurements, the test dose value used was 100 s consistent with recommended values (Mahan et al., 2023). However, multiple grains were rejected due to low signal-to-noise ratio (Figure 3.6). This means that the number of $D_e$ values being accepted is lower leading to less precise and potentially inaccurate ages.

To combat this, higher test doses were used to try and return more grains yielding $D_e$ values. Test doses were increased by 100 s each time. Interestingly, despite both sampling sites being close to one another geographically (~6 km), higher test dose values were required to separate observable luminescence signal from background noise. It was found the optimal test dose needed for BGR samples was 300 s, while the optimal test dose required to return some WCP $D_e$ values was 400 s.

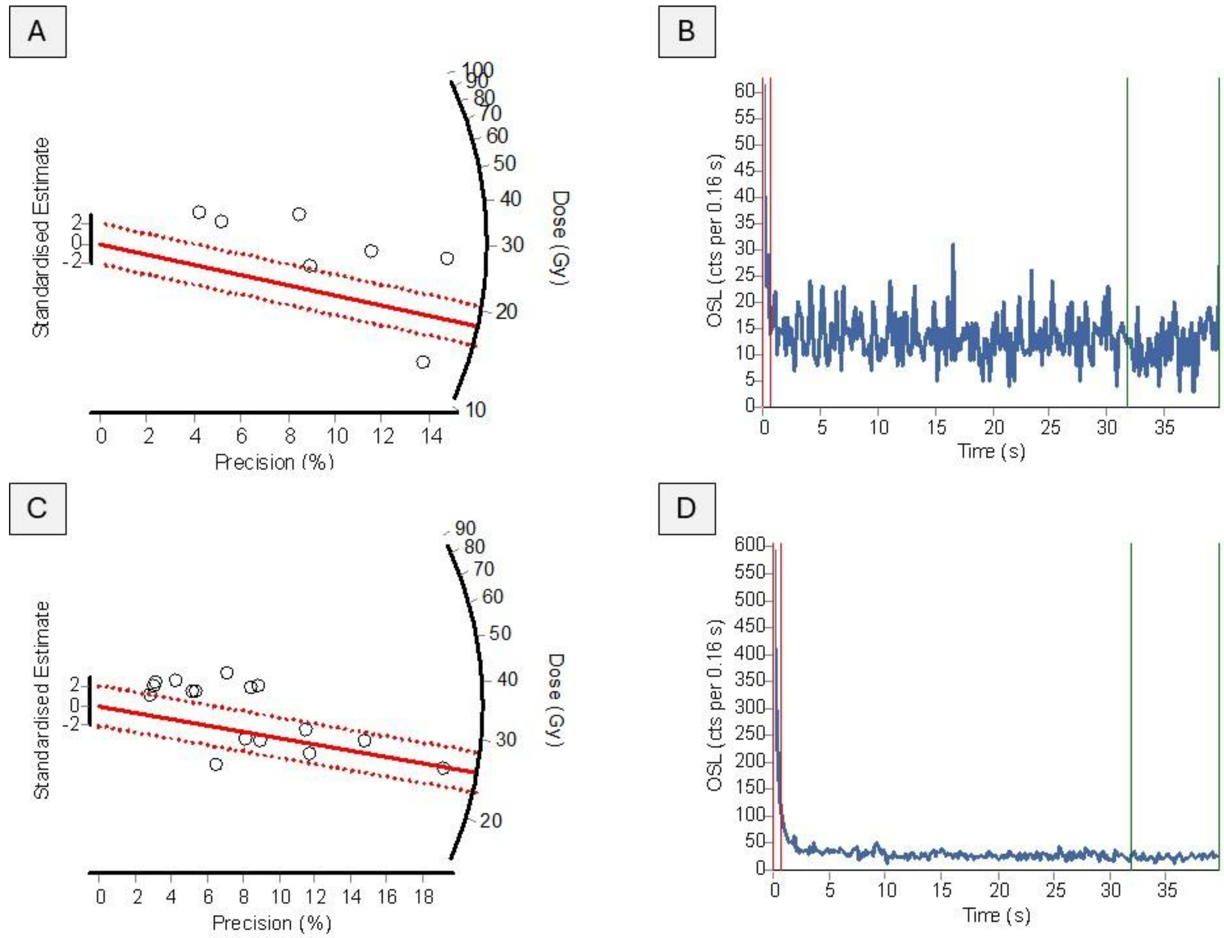


**Figure 3.6:** Comparison of radial plots from the same sample (25BGR-06), but with different test doses. **A)** Radial plot showing initial $D_e$ determination using a 100 s test dose. **B)** Low signal to background noise making $D_e$ determination for this sample difficult. **C)** Radial plot with an increased 300 s test dose. **D)** Test dose signal measured way above background level, making $D_e$ determination possible.

It was revealed that by increasing the test dose we were able to better analyze and characterize the ages using a radial plot. Radial plots showed that there were two distinct sets of $D_e$ values, which can provide potential ages of the CPR.

### 3.2.8 Environmental Dose Rate Measurements

The environmental dose rate ($D_r$, typically expressed in Gy/ka) is the other required component to determining an age of a feature using OSL, as discussed in Section 3.1.1. The environmental dose rate is the rate at which ionizing radiation is deposited into the mineral grains from the decay of $^{235}U$, $^{238}U$, $^{232}Th$, $^{87}Rb$, and $^{40}K$ in mineral grains and cosmic sources during the burial period (Rhodes, 2011). Samples were treated using the preparation methods described in step 2 in Section 3.2.1

The environmental dose rates for quartz minerals were calculated using the DRAC dose rate calculator from Durcan et al. (2015) (Table 3.3). Radionuclide conversion factors from Cresswell et al. (2018) were used for dose rate calculations. The grain size attenuation factor for the beta dose rate was selected after Guérin et al. (2012), and the cosmic dose rate was based on Prescott and Hutton (1994). The water content was assessed by comparing the mass of the sample before the drying cycle and after when the sample was left in a 50°C oven overnight and was measured to be weight stable. In the mix dose rate calculations used for these samples, both alpha and beta dose rates come from only <2 mm sieve fractions. For the gamma dose rate though, both sieve fraction proportions contribute to dose rate calculations and are normalized by their weight (Softa et al., 2021). However, it was found that the radionuclide concentrations for both sieve fractions were similar; or at the very least, had a negligible difference between them. Since this difference was negligible, the <2 mm sieve fraction was used for all dose rate calculations. Interestingly, based on initial conservative estimates for water content, the range for dose rate values were upwards of 4.5-5 Gy/ka as opposed to the 1-2 Gy/ka expected of deposits in these types of environments (Mahan et al., 2023). When water content percentages were then increased to 10 ± 10%, dose rate significantly decreased, indicating that field moisture was potentially not observed properly using methods described above.

**Table 3.3:** Radionuclide concentrations from ICP-MS/-AES and dose rate calculations for quartz minerals.

| Sample Name | Latitude & Longitude | Elevation (m) | Grain Size (µm) | Cosmic Dose Rate (Gy/ka) | Depth of Overburden (cm) | Water Content (%) | U (ppm) | Th (ppm) | K (%) | Rb (ppm) | Dose Rate (Gy/ka) |
|---|---|---|---|---|---|---|---|---|---|---|---|
| 25BGR-01 | N 47°29.670', W 114°35.684' | 878 | 125-180 | 0.268 ± 0.027 | 20 | 10 ± 10 | 3.59 ± 0.36 | 14.8 ± 0.74 | 3.06 ± 0.15 | 164 ± 8.2 | **4.73 ± 0.33** |
| 25BGR-02 | N 47°29.670', W 114°35.684' | 878 | 125-180 | 0.268 ± 0.027 | 25 | 10 ± 10 | 3.45 ± 0.35 | 13.9 ± 0.70 | 2.65 ± 0.13 | 142 ± 7.1 | **4.28 ± 0.34** |
| 25BGR-06 | N 47°29.670', W 114°35.684' | 878 | 125-180 | 0.268 ± 0.027 | 30 | 10 ± 10 | 3.29 ± 0.33 | 12.9 ± 0.65 | 2.59 ± 0.13 | 137 ± 6.9 | **4.14 ± 0.33** |
| 25WCP-01 | N 47°32.869', W 114°35.440' | 985 | 125-180 | 0.274 ± 0.027 | 25 | 10 ± 10 | 3.27 ± 0.33 | 12.3 ± 0.62 | 3.26 ± 0.16 | 136 ± 6.8 | **4.72 ± 0.38** |
| 25WCP-08 | N 47°32.869', W 114°35.440' | 985 | 125-180 | 0.274 ± 0.027 | 30 | 10 ± 10 | 3.55 ± 0.36 | 13.6 ± 0.68 | 3.16 ± 0.16 | 158 ± 7.9 | **4.77 ± 0.38** |
| 25WCP-21 | N 47°32.869', W 114°35.440' | 985 | 125-180 | 0.274 ± 0.027 | 30 | 10 ± 10 | 3.41 ± 0.34 | 12.3 ± 0.62 | 2.98 ± 0.15 | 144 ± 7.2 | **4.49 ± 0.36** |

### 3.2.9 Equivalent Dose Data

The equivalent dose data measured, following steps in Section 3.2.3, is represented using an Abanico plot, which is a combination of a radial plot and kernel density curve (Dietze et al., 2016). The Abanico plot was created by using the default R function call "plot_AbanicoPlot(…)" provided with the R package, "Luminescence" (Dietze et al., 2016; Dietze et al., 2025). $D_e$ results were calculated based on 125-180 µm quartz measurements, which were measured on the Risoe TL/OSL DA-20 reader described in Section 3.2.3 above.

Abanico plots were made to visualize the distribution of $D_e$ values for each sample. The plot consists of two separate parts. A radial plot on the left-hand side shows standard estimates in relation to precision, and a univariate plot on the right-hand side which shows the age frequency distribution (Dietze et al., 2016). An example of an Abanico plot with the different components is shown in Figure 3.7 which was created using example data provided with R package "Luminescence." For the bivariate part of the plot, the dark gray shaded area in the middle of the plot represents the dispersion bar for the dataset, the hatched line in the center of the plot represents the central age value, the two outside lines represent the boundaries of the values, the dots are the various $D_e$ values, and the lines on the inside represent the isochron (Duller, 2015). The right-hand side of the plot is represented by the univariate plot, which is a curved line showing the KDE curve. The KDE curve depicts the empirical estimate of the density function of the distribution that was measured (Galbraith and Roberts, 2012). Because of the wide variation in $D_e$ values (Figure 3.8), a minimum age model (MAM) (Galbraith et al., 1999) was selected to account for the variation in distributions. Aliquots that displayed grains having large distributions of saturation were removed from the analysis (Section 3.2.6) and then ran through the central age model (CAM, Galbraith et al., 1999). Since distributions paint an unclear picture about the distribution of $D_e$ values and put question as to the accuracy of the MAM, the CAM is another tool that was used to estimate the burial dose of samples analyzed.

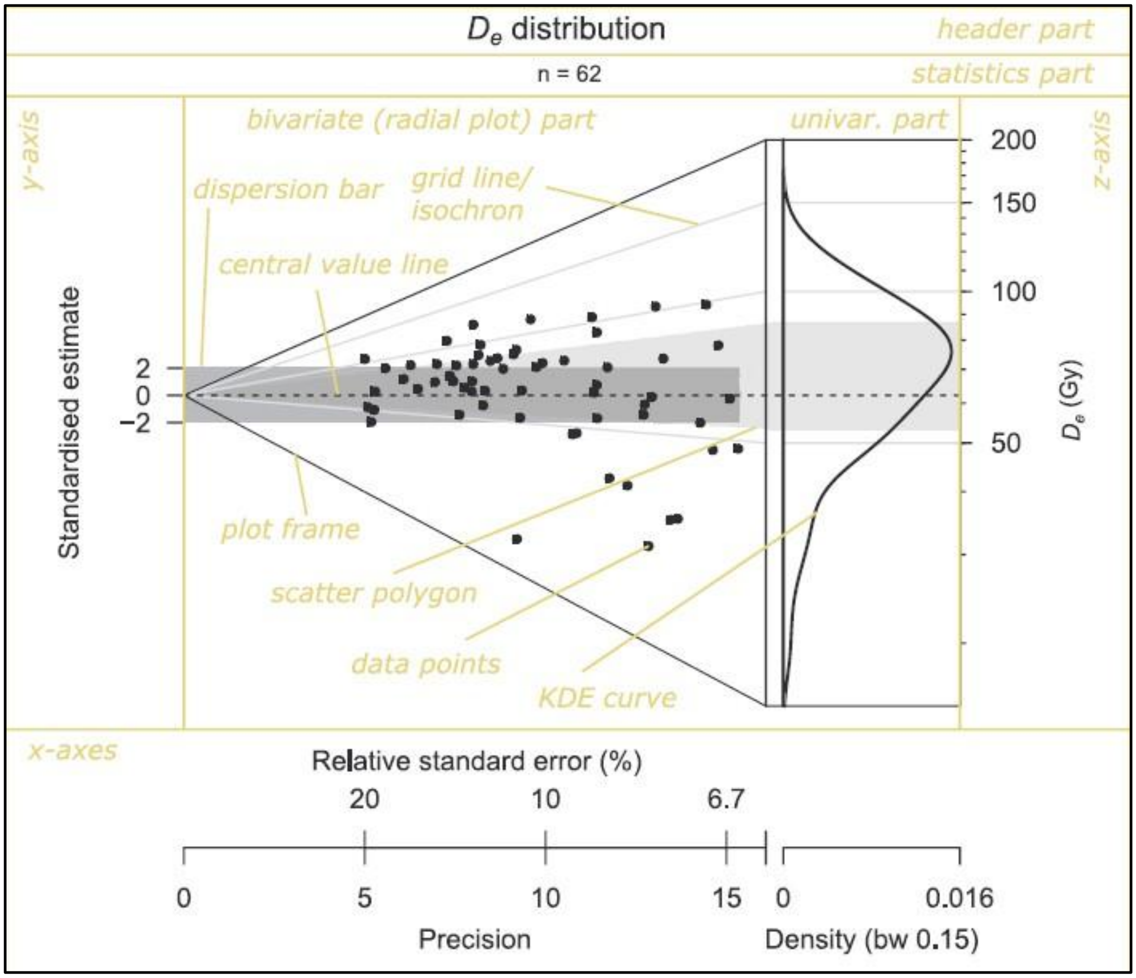


**Figure 3.7:** The Abanico plot as created by the default R function call (plot_AbanicoPlot(…)) using example data provided by with the R package "Luminescence." The plot consists of a two-part bivariate plot on the left side and a univariate plot on the right side (after Dietze et al., 2016).

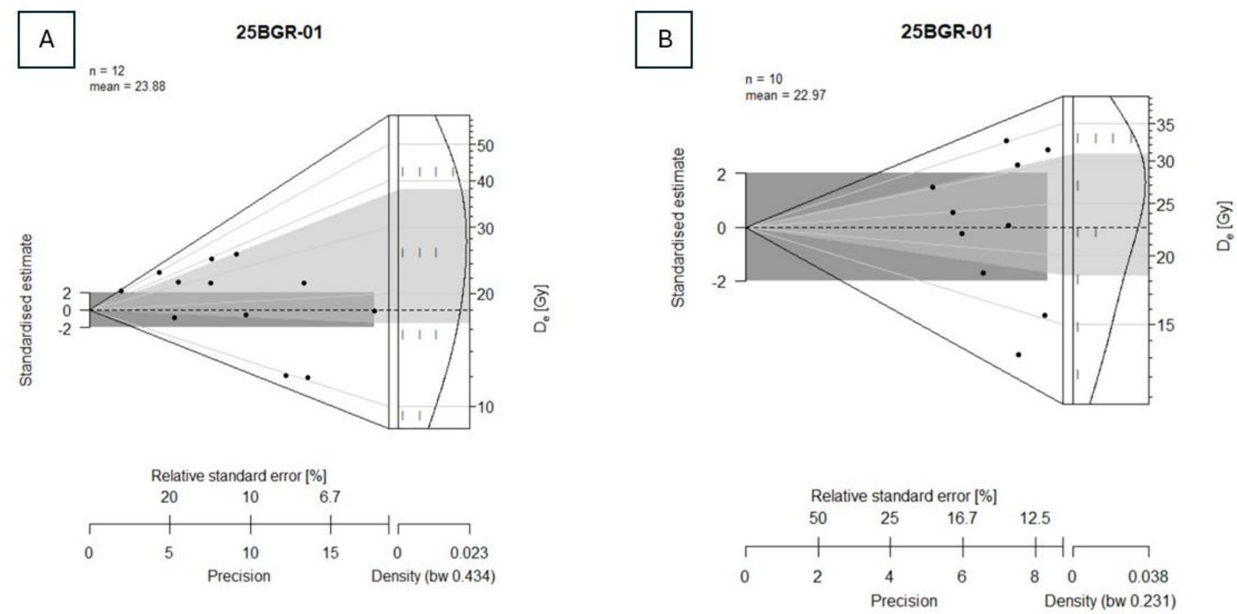


**Figure 3.8:** Abanico plots from 25BGR-02. (A) Aliquots containing grains that are in saturation are included in the distribution causing a broad range making estimates unclear. (B) When saturated grains are removed from the distribution following the $D_e/2D_0$ examination methodology described by Spencer and Robinson (2008), distributions show a more distinct peak indicating a mean $D_e$ value.

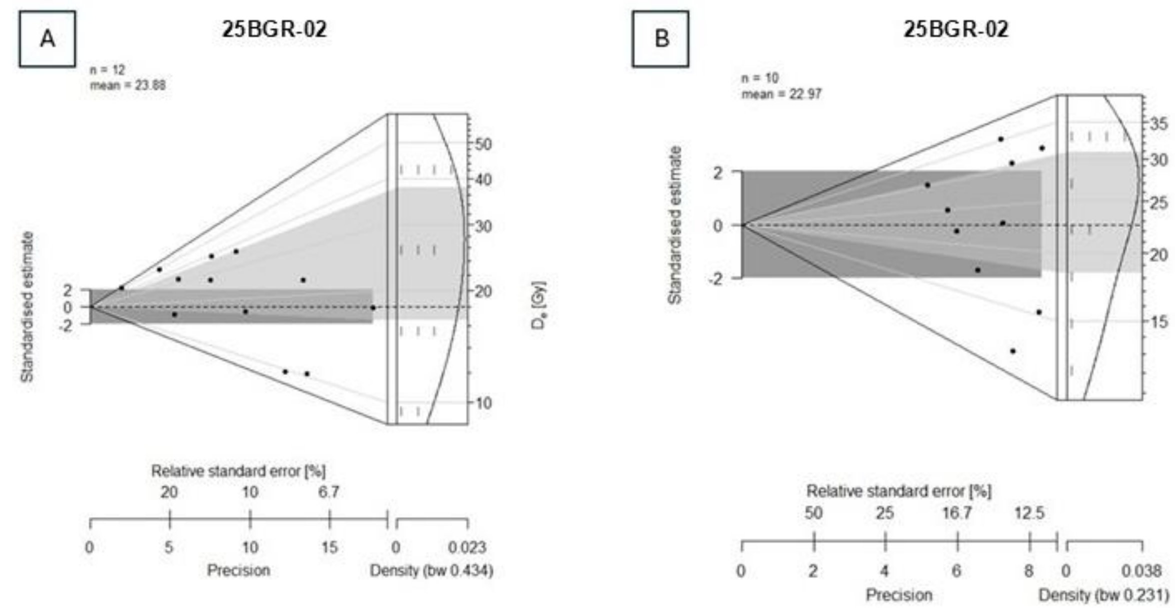


**Figure 3.9:** Abanico plots from 25BGR-02. (A) Aliquots containing grains that are in saturation are included in the distribution causing a broad range making estimates unclear. (B) When saturated grains are removed from the distribution following the $D_e/2D_0$ examination methodology described by Spencer and Robinson (2008), distributions show a more distinct peak indicating a mean $D_e$ value.

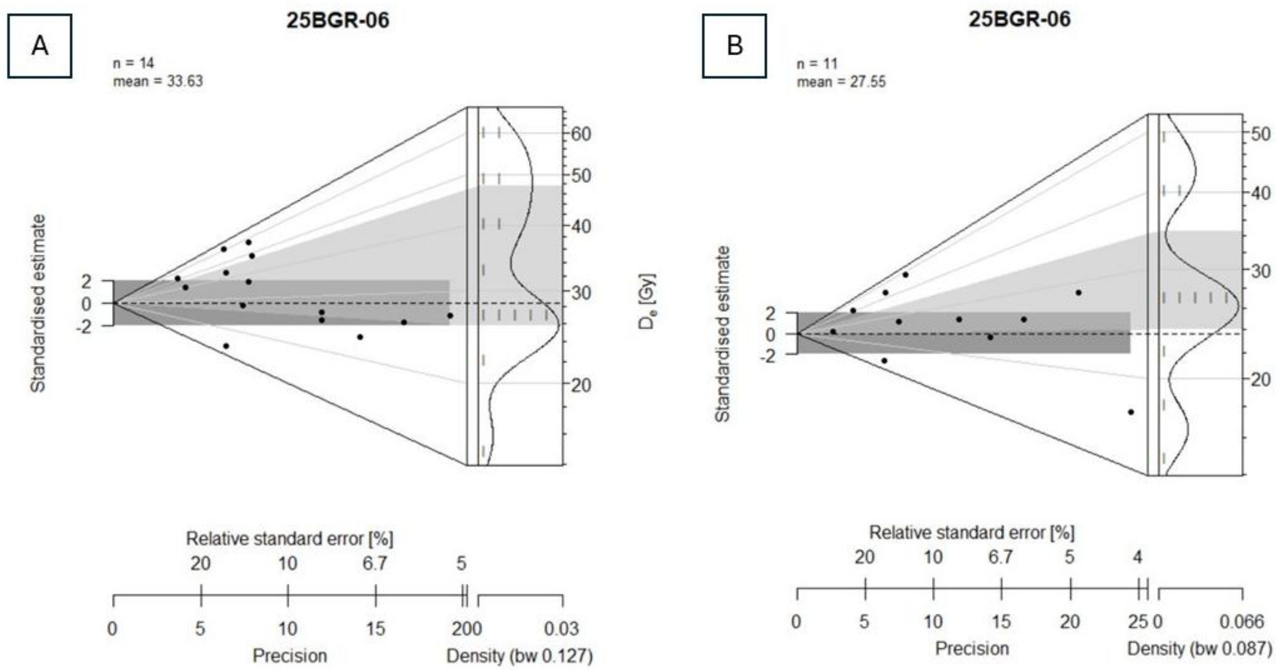


**Figure 3.10:** Abanico plots from 25BGR-02. (A) Aliquots containing grains that are in saturation are included in the distribution causing a broad range making estimates unclear. (B) When saturated grains are removed from the distribution following the $D_e/2D_0$ examination methodology described by Spencer and Robinson (2008), distributions show a more distinct peak indicating a mean $D_e$ value.

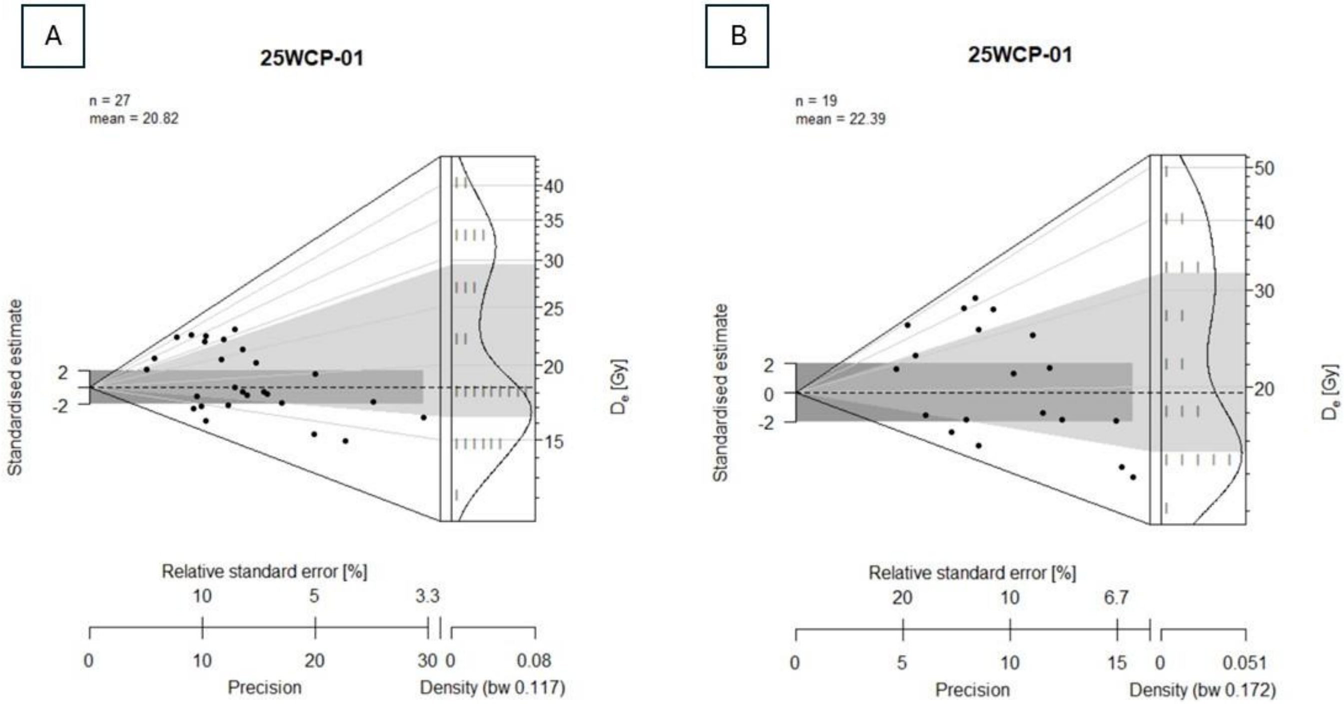


**Figure 3.11:** Abanico plots from 25BGR-02. (A) Aliquots containing grains that are in saturation are included in the distribution causing a broad range making estimates unclear. (B) When saturated grains are removed from the distribution following the $D_e/2D_0$ examination methodology described by Spencer and Robinson (2008), distributions show a more distinct peak indicating a mean $D_e$ value.

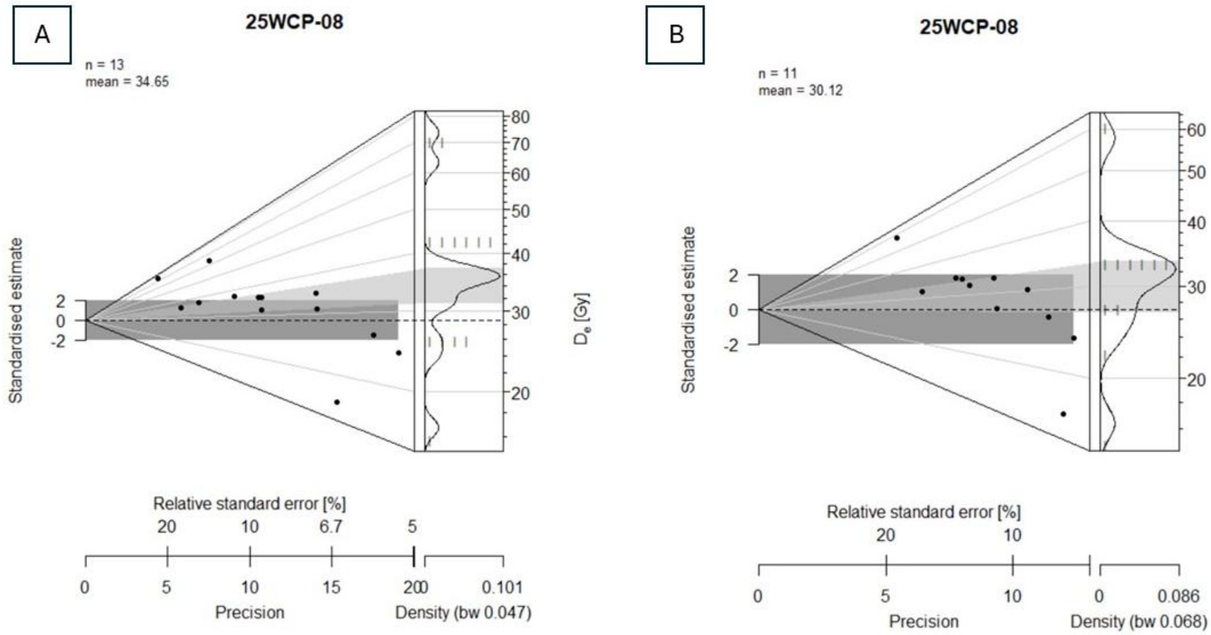


**Figure 3.12:** Abanico plots from 25BGR-02. (A) Aliquots containing grains that are in saturation are included in the distribution causing a broad range making estimates unclear. (B) When saturated grains are removed from the distribution following the $D_e/2D_0$ examination methodology described by Spencer and Robinson (2008), distributions show a more distinct peak indicating a mean $D_e$ value.

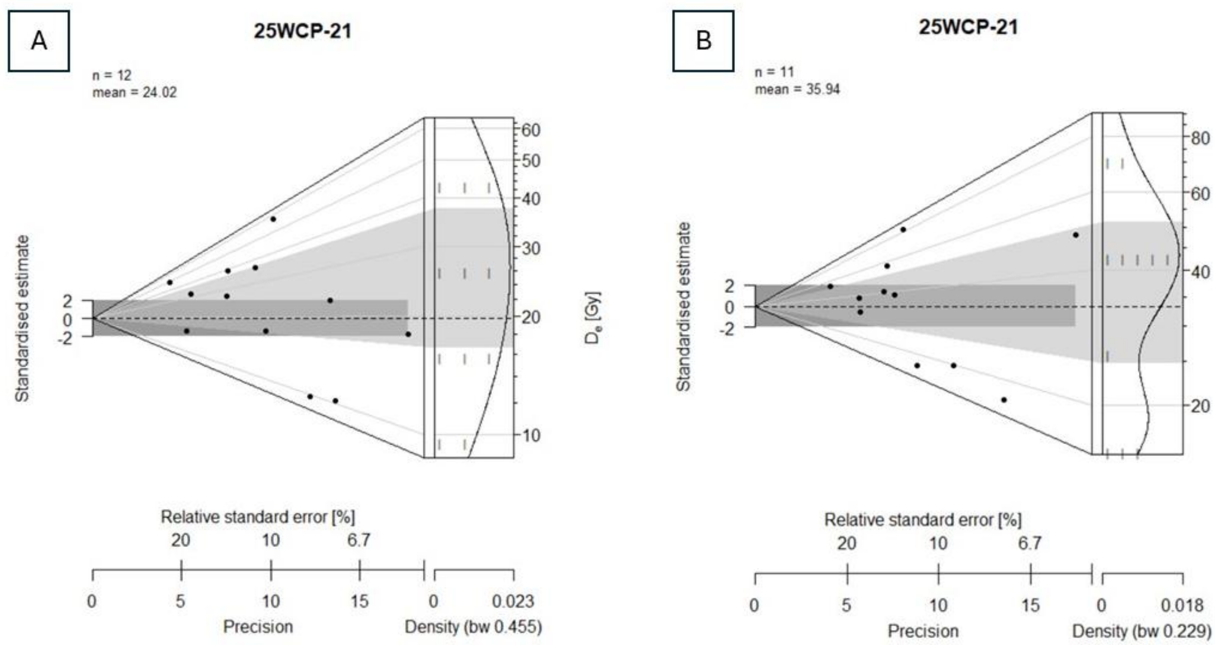


**Figure 3.13:** Abanico plots from 25BGR-02. (A) Aliquots containing grains that are in saturation are included in the distribution causing a broad range making estimates unclear. (B) When saturated grains are removed from the distribution following the $D_e/2D_0$ examination methodology described by Spencer and Robinson (2008), distributions show a more distinct peak indicating a mean $D_e$ value.

### 3.2.10 OSL Age Calculation

Incomplete zeroing of grains, like those found in glacial, fluvial, and alluvial environments, can produce a skewed distribution of dose values with higher values causing an extended high value tail (Rhodes, 2011). The MAM is a statistical method used to determine the age of samples that were not fully bleached prior to deposition which would lead some grains to yield larger $D_e$ signals and therefore ages (Galbraith et al., 1999). The model considers that partially bleached grains will have larger paleodoses, causing two distinct groups of differing $D_e$ values. The lower of these two groups of data should be approximately the same value as the data of the grains that have been fully bleached (Galbraith et al., 1999). This model is typically employed in environments where conditions do not allow for the proper resetting or bleaching of grains, particularly glacial environments. In glaciofluvial environments, grains are typically not zeroed properly due to these environments being highly energetic and turbid in terms of transport, have little light exposure, and rapid depositional processes (Rhodes, 2011). Because of this, the MAM can be a more robust method of determining the $D_e$ since it can account for any skew or wide variation in dose values (Arnold et al., 2009; Medialdea et al., 2014).

The CAM operates under the assumption that if $D_e$ values are normally distributed, then the mean value of the data set represents the true values of the data set, and the standard deviation is the standard deviation of dose values (Galbraith et al., 1999). While the CAM is typically applied to environments where grains are fully bleached prior to deposition, if grains that are in saturation are removed from the data set using $D_e/2D_0$ methodology described in earlier sections (Spencer and Robinson, 2008), this could provide another possible estimate of the burial dose.

In total, 10 samples were analyzed for age data from the Camas Prairie Ripples. Out of these, seven of the samples that were analyzed by running them through the MAM and CAM (Table 3.3). Due to dose distributions showing inconclusive results on what model would be most effective, it should be noted that the ages calculated in this study should not be reflective of true burial ages. Nonetheless, they are still listed in Table 3.4, since it serves as a first step towards dating these complex features by providing information about the potential ages of these features and number of flooding events that caused these feature's formation.

**Table 3.4:** Calculated ages based on determined $D_e$ and dose rate values.

| Sample | Dose Rate (Gy/ka) | $D_e$ (Gy) CAM | CAM Age (ka) | Overdispersion (%) | $D_e$ (Gy) MAM | MAM Age (ka) |
|---|---|---|---|---|---|---|
| 25BGR-01 | 4.73 ± 0.38 | 22.3 ± 2.8<br>n = 10 | **4.71 ± 0.70** | 41.2 ± 1.7 | 16.3 ± 0.3 | **3.46 ± 0.28** |
| 25BGR-02 | 4.28 ± 0.34 | 28.4 ± 2.7<br>n = 14 | **6.63 ± 0.84** | 42.5 ± 2.3 | 23.7 ± 0.3 | **5.53 ± 0.45** |
| 25BGR-06 | 4.14 ± 0.33 | 27.5 ± 3.2<br>n = 12 | **6.64 ± 0.94** | 31.2 ± 2.1 | 23.3 ± 0.4 | **5.63 ± 0.46** |
| 25WCP-01 | 4.72 ± 0.38 | 22.2 ± 2.1<br>n = 19 | **4.71 ± 0.70** | 40.3 ± 1.6 | 16.9 ± 0.5 | **3.58 ± 0.31** |
| 25WCP-08 | 4.77 ± 0.38 | 29.7 ± 2.5<br>n = 11 | **6.23 ± 0.73** | 25.3 ± 2.0 | 24.9 ± 0.6 | **5.22 ± 0.44** |
| 25WCP-21 | 4.49 ± 0.36 | 30 ± 5.5<br>n = 11 | **6.68 ± 1.34** | 45 ± 3.7 | 17.3 ± 0.4 | **3.85 ± 0.32** |

# Chapter 4 - Discussion

The main aim of this study was to attempt to use established OSL techniques on quartz mineral grains from samples collected from the crest of three giant current ripples from the Camas Prairie Ripples in northwestern Montana and determine a minimum depositional age. Given the largely clast-supported gravelly, cobbly, and bouldery architecture of the ripples (e.g., Figs. 2.6, 2.8, and 2.10), stainless steel tube sampling was not possible, and for the most part the samples collected were excavated samples of sediment matrix from the trench walls. Samples were collected at increasing stratigraphic depth within each ripple to potentially identify multiple flooding events following Kalińska et al. (2025).

Based on previous studies that have investigated the chronology of different flooding events identified in the greater Channeled Scablands area from northwestern Montana to Washington and Oregon, we would expect ages for these features to fall into the range from approximately 13.7 to 21 ka (Amidon and Clark, 2015; Benito and O'Connor, 2003; Hanson and Clague, 2016; Smith et al., 2018; Smith et al., 2022). For the luminescence studies conducted in northwestern Montana, with consideration for the different lake level fluxes and differing flood deposits, acute partial bleaching of quartz sand grains remains a critical issue (Hanson et al., 2012; Smith et al., 2018; Smith et al., 2022). However, preliminary OSL studies from the two tube samples we were able to collect from trench BGR showed quartz data that suggested established OSL analyses on quartz grains could be successful (see Figure 3.3 (B) in Chapter 3) under the assumption that typical dose rates in these types of environments range from 1-2 Gy/ka (Mahan et al., 2023), leading us to focus on quartz grains for further age determination. However, because of the widespread nature of the data in all of the Abanico plots and overdispersion in the data set, the ages found are likely to be apparent ages instead of true burial ages. We use the term *apparent ages* for ages that are raw, calculated ages factoring in partially bleached grains instead of fully bleached grains.

OSL dating analysis on the quartz from the sediment matrices collected from the trenches at the WCP and BGR localities yielded unexpected results. The MAM ages obtained in this study from the BGR locality ranged from 3 to 5 ka, and the ages obtained from the WCP locality ranged from approximately 3.5 to 5 ka. Ages obtained using the CAM model for the BGR and WCP localities ranged from 4.1 to 6.6 ka and 4.7 to 6.7 ka, respectively. This is significantly younger than other GLM deposits that have been directly dated in northwest Montana. The youngest age that has been dated in relation to the Missoula floods in the Glacier Peak Tephra with an age of 13.7 ka (O'Connor et al., 2020). The 10.6 age reported by Smith et al. (2018) represents lake level changes that would have taken place after outburst floods from GLM. While not directly related to the Missoula floods, this could represent GLM inundation after all flooding events could have occurred. This inundation could have provided a higher moisture content for the sediment, therefore affecting the dose rate, leading to a lower dose rate. Thus, the ages derived from the CAM appear to be slightly closer to expected ages than those determined using the MAM. Interestingly, ages obtained using the CAM would expected be much higher than those obtained using the MAM since the CAM is taking the average of all values including both really high and really low $D_e$ values.

One of the many potential reasons that the ages are severely underestimated (2.5-3x younger than expected) could be that there are malign properties of the quartz minerals analyzed in this study. One intrinsic property of this quartz that could be a clue to a malign property is that this quartz saturates earlier than typically expected. As discussed later, this could be caused by lithologies that the floods would have encountered from their source to the Camas Prairie Basin, since some lithologies have more suitable qualities for quartz than others. Another malign property is the low background to noise ratio characteristic. While the increase in test dose increased the chance of determining the $D_e$ value, the high test doses that needed to be incorporated to determine the $D_e$ values could have created a dose-dependent effect that shifts the whole distribution to lower doses or broadens the distribution of high to low doses than the true distribution. The thermal instability of quartz could also cause a shift towards lower dose distributions. When signals contain significant contributions from the thermally unstable components, then the distribution of values would show a decrease, leading to an underestimation of ages (Fan et al., 2011). It should be noted that Hanson et al. (2012) hypothesized it could be possible that their collected quartz data could be underestimated due to the influence of this unstable component in the luminescence signal. Additionally, as stated above, surrounding lithology could contribute to malign quartz characteristics. Quartz derived from volcanic deposits can yield underestimated ages because quartz from these deposits can fade anomalously similarly to feldspars (Tsukamoto et al., 2007). Based on prior geologic mapping, it has been found that there are sills and dikes in Camas Prairie region (Figure 1.2; Harrison et al., 1986) and modern GLM region (Scarberry, 2023). Some of these sills and dikes are Oligocene and Eocene in age. As mentioned previously, these rocks and subsequent sand grains from these rocks could have carried vast distances from the ice-lake margin and deposited into the Camas Prairie Basin while larger clasts could have been sourced proximal to the features. If quartz from these deposits were taken from the bedrock in transport and deposited, they could have poor characteristics that would allow them to not be accurately dated. Lastly, it is possible that the sampling setup of covering the trenches in tarp before collecting the sediment matrices before sampling could have inadvertently led to bleaching of grains by not providing dark enough conditions while sampling. Thus, causing underestimation in age values. More conventional tube sampling of quartz samples could reveal if this was the case or not. On top of this, it was found that by increasing the water content in dose rate calculations (10 ± 10%), it made the calculated dose rate drop significantly to dose rates expected by Mahan et al. (2023) for these types of environments. Field moisture is often one of the biggest uncertainties in dose rate calculation, so it is possible that the assessment of field moisture was not as accurately determined as previously thought. In this study, an experimental value of 10 ± 10% was used to account variation in moisture content throughout an entire year in the modern day. Something else to consider too is inundation of GLM. If GLM waters sat on top of the ripples, this pooling of water could have resulted in greater saturation, therefore lowering the influence of the beta dose rate and cosmogenic dose rate. Accounting for these two factors could potentially lower the dose rate values in this study to more expected results. Thus, yielded ages for these sand grains anywhere in the expected 13.7 to 21 ka.

Some underestimation could also arise from certain flaws in the statistical models. Quartz in tectonically active zones can have dim or insensitive characteristics. This is because as quartz-bearing bedrock is brought up to the surface and is eroded and only transported short distances, the quartz sand grains are geologically young and have limited history of dosing and bleaching cycles, effectively limiting their use to determine age estimates of features (Lawson et al., 2015; Rhodes, 2011). This results in underestimates of age using the MAM by only accounting for grains that are younger than the bulk of the deposit (Arnold et al., 2009). Another main reason that could cause underestimation of age is acute partial bleaching. While the MAM accounts for this by identifying the lowest dose population which represents the well bleached quartz grains (Galbraith et al., 1999), it has been shown that if there are grains that are sensitive to IR stimulation in an aliquot, then this can cause populations of grains with low $D_e$ to occur, and hence, lead to an underestimation of the depositional age (Olley et al., 2004). All of these factors combined could lead to an inaccurate age that were found analyzing these deposits with established OSL measurements on quartz sand grains. However, it may seem that there are some stratigraphic features that are identifiable despite the underestimation in age.

"The Great Scablands Debate" (O'Connor et al., 2020) is an area of ongoing research focused on determining an age and number of discrete flooding events that may have caused the formation of the Camas Prairie Ripples and the Channeled Scablands. The debate of how many flooding events may have caused these features, and the surrounding landscape is the more prevalent question that is being sought out to be debated and argued. Many hypotheses about how many floods that formed the Channeled Scablands, and the Camas Prairie have been argued since the identification of these features in the early 1900's. There are arguments along the spectrum for as many as 40 different floods (Waitt, 1980) to one cataclysmic flooding event first hypothesized by Joseph Pardee in 1942. Interestingly though, despite what we consider are underestimated ages, in both localities the samples collected deeper stratigraphically within the ripple features were of older estimated age than those found closer to the surface. If all of the age values have been shifted too young and underestimated, then this could indicate that there are records of multiple flooding events at increasing stratigraphic depth within the ripple and ripple feature. However, this could also be indicating a greater bleaching efficiency in proximity to the ripple crest. This may also indicate that there could be more flooding events that are recorded in the stratigraphy at increasing stratigraphic depth deeper in the ripple feature.

Possible future work for the Camas Prairie Basin and the Camas Prairie Ripples is vast. Analysis of feldspar sand grains could potentially yield more reliable ages since it has been shown that there have been better successes of dating features in glacial environments where quartz characteristics can be poor and have populations of grains that are incompletely bleached (Buylaert et al., 2012; Hanson and Clague, 2016). Smith et al. (2022) employed the use of observing the luminescence signal at depth within the upper centimeters of a cobble that was hypothesized to have been buried during outburst flooding near Alberton Gorge along the Clark Fork River. Based on the profile of the luminescence signal, they were able to discern cobbles that were well bleached and therefore, provide an age estimate (Figure 4.1). Cobbles for future studies were collected in this study and could be used to confirm or dispute ages already collected or found in this study. Additionally, making use of a more robust dating method like $^{10}Be/^{26}Al$ cosmogenic nuclide dating could negate the problem of partial bleaching, but it should be noted that there are potential challenges for using this method in glacial environments that are similar to luminescence methods (i.e. inheritance).

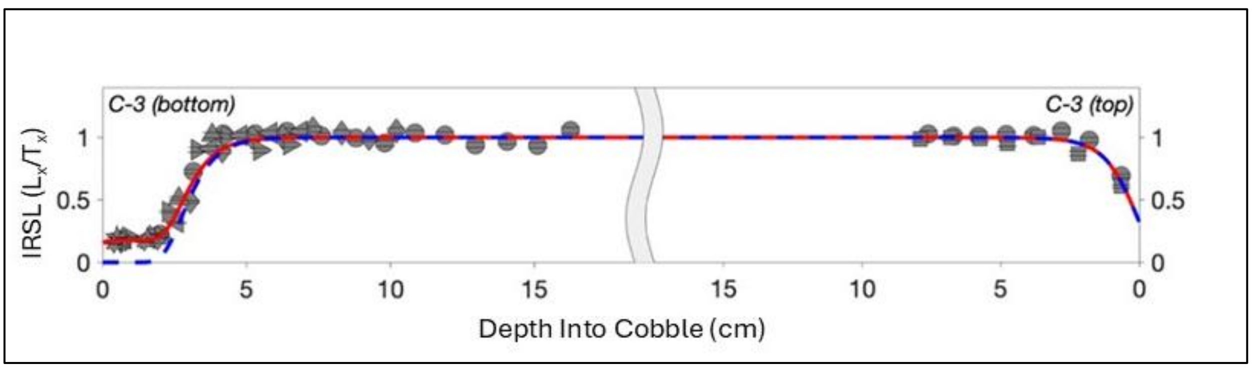


**Figure 4.1:** Modified plot of IRSL signals from the top and bottom of a cobble carried and buried by glacial outburst floods from Smith et al. (2022). A well bleached signal (left) shows a sigmoidal shape compared to a partially bleached signal (right). This method has the potential to determine burial ages of cobbles in environments where traditional OSL techniques could prove challenging.

On top of using different luminescence and cosmogenic methods, investigation of different notch systems in the Camas Prairie Basin like Rainbow Pass and Merkle Creek to compare age data found in this study could also prove useful. The examination of different localities displaying differing flood stages may also provide better bleaching conditions that allow for more routine luminescence measurements (Kalińska et al., 2025).

# Chapter 5 - Summary and Conclusion

The main aim of this study was to examine the Camas Prairie Ripples located in northwestern Montana by trying to determine the depositional age of these features and the number of discrete flooding events that may have caused these features. A total of 55 samples were collected from the three trenches in the Camas Prairie Basin. Using established OSL measurements on quartz sand grains, it was found that samples collected at the BGR locality had an age range of 3-5 ka, while the samples collected at the WCP locality had age range of 3.5-5 ka. Despite these likely underestimated ages, it was also found that there was a noticeable difference in age between samples collected closer to the ripple crest than those collected deeper at stratigraphic depth. This may indicate that multiple flooding events could be identified using other luminescence and cosmogenic methods.

Limitations to small-aliquot OSL quartz dating (i.e. partial bleaching, feldspar contamination, early dose saturation, and insensitive quartz characteristics) were encountered during this study. Other luminescence methods like OSL analysis on feldspars, rock surface luminescence, and $^{10}Be/^{26}Al$ cosmogenic nuclide dating may be able to circumvent these issues and provide a more reliable and accurate age (Jenkins et al., 2018; Smith et al., 2022; Smith et al., 2026). Future work could also include the examination of different notch systems, like Rainbow Pass and Markle Pass, to examine if ages found in those locations are concordant to those found in this study or support ages found for other features in other studies conducted in this region. Examination of all this information is critical to understanding the glacial history of the region and the greater Channeled Scablands.

# References


Aitken, M.J., 1985, Thermoluminescence Dating: Academic Press, London.

Alho, P., Baker, V., Smith, L., 2010, Paleohydraulic reconstruction of the largest Glacial Lake Missoula draining(s): Quaternary Science Reviews, v. 29, p. 3067-3078.

Amidon, W.H., Clark, A.C., 2015, Interaction of outburst floods with basaltic aquifers on the Snake River Plain: Implications for Martian canyons: *GSA Bulletin*, v. 127, i. 5/6, p. 688-701.

Arnold, L.J., Roberts, R.G., Galbraith, R.F., DeLong, S.B., 2009, A revised burial dose estimation procedure for optical dating of young and modern-age sediments: *Quaternary Geochronology*, v. 4, i., 4, p. 306-325.

Baker, V.R., Bunker, R.C., 1985, Cataclysmic late pleistocene flooding from Glacial Lake Missoula: A review: Quaternary Science Reviews, v. 4, p. 1-41.

Balbas A.M., Barth, A.M., Clark, P.U., Clark, J., Caffee, M., O'Connor, J., Baker, V.R., Konrad, K., Bjornstad, B., 2017, $^{10}$Be dating of late Pleistocene megafloods and Cordilleran Ice Sheet retreat in the northwestern United States: *Geology*, v. 45, n. 7, p. 583-586.

Batchelor, C.L., Margold, M., Krapp, M., Murton, D.K., Dalton, A.S., Gibbard, P.L., Stokes, C.R., Murton, J.B., Manica, A., 2019, The configuration of Northen Hemisphere ice sheets through the Quaternary: Nature Communications, v. 10, i. 3713, p. 1-10.

Benito, G., O'Connor, J.E., 2003. Number and size of last-glacial Missoula floods in the Columbia River valley between the Pasco Basin, Washington, and Portland, Oregon: GSA Bulletin, v. 115, i. 5, p. 624-638.

Blair, T.C., McPherson, J.G., 1999, grain-size and textural classification of coarse sedimentary particle: *Journal of Sedimentary Research*, v. 69, i. 1, p. 6-19.

Bohoroquez P., Cañada-Pereira P., Jimenez-Ruiz, P.J., del Moral-Erencia J.D., 2019, The fascination of shallow-water theory for the formation of megaflood-scale dunes and antidunes: Earth Science Reviews, v. 193, p. 91-108.

Booth, D.B., Troost K.G., Clauge, J.J., Waitt, R.B., 2004, The Cordilleran Ice Sheet: Developments in Quaternary Science, v. 1, p. 17-43.

Bøtter-Jensen, L., Mckeever, Stephen, Wintle, A.G., 2003, Chapter 1. Introduction.

Buylaert, J.P., Jain, M., Murray, A.S., Thomsen, K.J., Thiel, C., Sohbati, R., 2012, A robust feldspar luminescence dating method for Middle and Late Pleistocene sediments: *Boreas*, v. 41, p. 435-451.

Carling, P.A., 1999, Subaqueous gravel dunes: *Journal of Sedimentary research*, v. 69, i. 3, p. 534-545.

Chapot, M.S., Duller, G.A.T., Barham, L.S., 2022, Challenges of dating quartz OSL samples with saturated grains: Lessons from single-grain analyses of low dose-rate samples from Victoria Falls, Zambia: *Quaternary Geochronology*, v. 72, p. 1-9.

Clark, P.U., Gyke, A.S., Shakun, A., Clark, J., Mitrovica, J., Hostetler, S., McCabe, M.A., 2009, The Last Glacial Maximum: *Science*, v. 325 , n. 5941, p. 710-714.

Clarke, G.K.C., Mathews, W.H., Pack, R.T., 1984, Outburst Floods from Glacial Lake Missoula: Quaternary Research, v. 22., i. 3, p. 289-299.

Cresswell, A.J., Carter, J., Sanderson, D.C.W., 2018, Dose rate conversion parameters: Assessment of nuclear data: *Radiation Measurements, v.* 120, p. 195-201.

Dalton, A.S., et al., 2020, An updated radiocarbon-based ice margin chronology for the last deglaciation of the North American Ice Sheet Complex: Quaternary Science Reviews, v. 234, i. 106223, p. 1-27.

DeLong, S.B., Arnold, A.J., 2007, Dating alluvial deposits with optically stimulated luminescence, AMS 14C and cosmogenic techniques, western Transverse Ranges, California, USA: Quaternary Geochronology, v. 2, p. 129-136.

Dietze, M., Kreutzer, S., Burow, C., Fuchs, M.C., Fischer, M., Schmidt, C., 2016, The abanico plot: Visualizing chronometric data with individual standard errors: *Quaternary Geochronology*, v. 31, p. 12-18.

Dietze, M., Kreutzer, S., 2025. plot_AbanicoPlot(): Function to create an Abanico Plot.. Function version 0.1.20. In: Kreutzer, S., Burow, C., Dietze, M., Fuchs, M.C., Schmidt, C., Fischer, M., Friedrich, J., Mercier, N., Philippe, A., Riedesel, S., Autzen, M., Mittelstrass, D., Gray, H.J., Galharret, J., Colombo, M., Steinbuch, L., Boer, A.d., 2025. Luminescence: Comprehensive Luminescence Dating Data Analysis. R package version 1.1.2. https://r-lum.github.io/Luminescence/

Duller, G.A.T., 2015, The Analyst software package for luminescence data: overview and recent improvements: *Ancient TL*, v. 33, n. 1, p. 35-42.

Durcan J.A., King, G.E., Duller, G.A.T., 2015, DRAC: Dose Rate and Age Calculator for trapped charge dating: *Quaternary Geochronology*, v. 28, p. 54-61.

Dyke, A.S., 2004, An outline of North American deglaciation with emphasis on central and northern Canada, in Ehlers, J. and Gibbard, P.L. eds., Developments in Quaternary Sciences, Elsevier, Quaternary Glaciations-Extent and Chronology, v. 2, p. 373–424.

Emmer et al., 2022, Progress and challenges in glacial lake outburst flood research (2017-2021): a research community perspective: *Natural Hazards and Earth Science Systems*, v. 22, i. 9, p. 3041-3061.

Faershtein, G., Porat, N., Matmon, A., 2019, Natural saturation of OSL and TT-OSL signals of quartz grains from Nilotic origin: *Quaternary Geochronology*, v. 49, p. 146-152.

Folk, R.L., Andrews, P.B., Lewis, D.W., 1970, Detrital sedimentary rock classification and nomenclature for use in New Zealand: *New Zealand Journal of Geology and Geophysics*, v. 13, i. 4, p. 942.

Fan, A., Li, S., Li, B., 2011, Observation of unstable fast component of quartz: *Radiation Measurements*, v. 46, p. 21-28.

Fraser, K.I., Enkelmann, E., Jess, S., Gilber, H., Grieco, R., 2021, Resolving the Cenozoic History of Rocky Mountain Exhumation Along the Central Rocky Mountain Trench Using Apatite Low-Temperature Thermochronology: Tectonics, v. 40, i. 10, p. 1-25.

Fuchs, M., Owen, L.A., 2008, Luminescence dating of glacial and associated sediments: review, recommendations and future directions: Boreas, v. 37, i. 4, p. 636-659.

Galbraith, R.F., Roberts, R.G., 2012, Statistical aspects of equivalent dose and error calculation and display in OSL dating: An overview and some recommendations: *Quaternary Geochronology*, v. 11, p. 1-27.

Galbraith, R.F., Roberts, R.G., Laslett, G.M., Yoshida, H., Olley, J.M., 1999, Optical Dating of Single and Multiple Grains of Quartz from Jinmium Rock Shelter, Northern Australia: Part 1, Experimental Design and Statistical Models: Archaeometry, v. 41, i. 2, p. 339-364.

Guérin, G., Mercier, N., Nathan, R., Adamiec, G., Lefrais, Y., 2012, On the use of the infinite matrix assumption and associated concepts: A critical review: *Radiation Measurements*, v. 47, p. 778-785.

Hanson, M., Clague, J., 2016, Record of glacial Lake Missoula floods in glacial Lake Columbia, Washington: Quaternary Science Reviews, v. 133, p. 62-76.

Hanson, M.A., Lian, O.B., Clague, J.J., 2012, The sequence and timing of large late Pleistocene floods from glacial Lake Missoula: Quaternary Science Reviews, v. 31, p. 67-81.

Harrison J.E., Griggs, A.B., Wells, J.D., 1986, Geologic and structure maps of Wallace 1 degree x 2 degrees quadrangle Montana and Idaho: U.S. Geological Survey and Miscellaneous Investigations Series Map I-1509-A, scale 1:250,000.

Harrison, S., Kargel, J.S., Huggel, C., Reynolds, J., Shugar, D.H., Betts, R.A., Emmer, A., Glasser, N., Haritashya, U.K., Klimes, J., Schaub, Y., Wiltshire, A., Regmi, D., Vilímek, 2018, Climate change and the global pattern of moraine-dammed glacial lake outburst floods: *The Cryosphere*, v. 12, i. 4, p. 1195-1209.

Hendy, I., 2009, A fresh perspective on the Cordilleran Ice Sheet: Geology, v. 37, i. 1, p. 95-96.

Hofmann, M.H., Hendrix, M.S., Sperazza, M., Moore, J.N., 2006, Neotectonic evolution and fault geometry change along a major extensional fault system in the Mission and Flathead Valleys, NW-Montana: *Journal of Structural Geology*, v. 28, i. 7, p. 1244-1260.

Kalińska E., Weckwerth P., Alexanderson, H., Piotrowski, J., Wysota W., 2025, OSL dating of glacial outburst flood deposits in NE Poland and their bleaching problem inferred from the landform-sediment associations and regional context: *Quaternary Research*, v. 124, p. 26-46.

Krbetschek, M.R., Götze, J., Dietrich A., Trautmann, T., 1997, Spectral information from minerals relevant for luminescence dating: Radiation Measurements, v. 27, i. 5, p. 695-748.

Lawson, M.J., Daniels, J.T.M., Rhodes, E., 2015, Assessing Optically Stimulated Luminescence (OSL) signal contamination within small aliquots and single grain measurements utilizing the composition test: *Quaternary International*, v. 362, p. 34-41.

Lee, K., 2009, Catastrophic Flood Features at Camas Prairie, Montana: Colorado School of Mines, p. 1-39.

Lister, J.C., 1975, The Sedimentology of Camas Prairie Basin and its Significance to the Lake Missoula Floods [Master's thesis]: University of Montana, 1-66.

Mahan, S.A., et al., 2023, Guide for interpreting and reporting luminescence dating results: *GSA Bulletin*, v. 135, n. 5/6, p. 1480-1502.

Mauk, J.L., 1983, Stratigraphy and Sedimentation of the Proterozoic Burke and Revett Formations, Flathead Reservation, Western Montana [Master's thesis]: University of Montana, 1-58.

Medialdea, A., Thomsen, K.J., Murray, A.S., Benito G., 2014, Reliability of equivalent-dose determination and age-models in the OSL dating of historical and modern paleoflood sediments: *Quaternary Geochronology*, v. 22, p. 11-24.

Murray, A.S., Wintle, A.G., 2000. Luminescence dating of quartz using an improved single-aliquot regenerative-dose protocol. Radiation measurements 32, 57–73.

Murray, A.S., Wintle, A.G., 2003. The single aliquot regenerative dose protocol: potential for improvements in reliability. Radiation measurements 37, 377–381.

O'Connor, J.E., Baker, V.R., Waitt, R.B., Smith, L.N., Cannon, C.M., George, D.L., Denlinger R.P., 2020, The Missoula floods-A review of ice-age megafloods in the Columbia River basin: Earth-Science Reviews, v. 208, i. 103181, p. 1-52.

Olley, J.M., Pietsch, T., Roberts, R.G., 2004, Optical dating of Holocene sediments from a variety of geomorphic settings using single grains of quartz: *Geomorphology*, v. 60, p. 337-258.

Pardee J., 1942, Unusual Currents in Glacial Lake Missoula, Montana. Bulletin of the Geological Society of America: v. 53, i. 11, p. 1570-1599.

Porat, N., 2006, Use of magnetic separation for purifying quartz for luminescence dating: Ancient TL, v. 24, n. 2, p. 33-36.

Porter, S.C., 2004, Glaciation of western Washington, U.S.A.: *Developments in Quaternary Science*, v. 2, Part B., p. 289-293.

Prescott J.R., Hutton J.T., 1994, Cosmic ray contributions to dose rates for luminescence and ESR dating: Large depths and long-term time variations: *Radiation Measurements*, v. 23, i. 2-3, p. 497-500.

Quirk, B.J., Huss, E., Laabs, B.J.C., Leonard, E., Licciardi, J., Plummer, M.A., Caffee, M.W., 2022, Late Pleistocene glacial chronologies and paleoclimate in the northern Rocky Mountains: *Climate of the Past*, v. 18, i. 2, p. 293-312.

Rhodes, E., 2011, Optically Stimulated Luminescence Dating of Sediments over the Past 200,000 Years: Annual Review of Earth and Planetary Sciences, v. 39, p. 462-488.

Rosenblum, S., 1958, Magnetic susceptibilities of minerals in the Frantz Isodynamic magnetic separator: American Mineralogist, v. 43, n. 1-2, p. 170-173.

Şahiner, E., Meriç, Polymeris, G.S., 2014, Assessing the impact of IR stimulation at increasing temperatures to the OSL signal of contaminated quartz: Radiation Measurements, v. 68, p. 14-22.

Scarberry, K.C., 2023, Geologic map of the Hubbart Reservoir 7.5' quadrangle, Flathead and Sanders Counties, Montana: Montana Bureau of Mines and Geology, GM 92, scale 1:24,000.

Smith L., 2006, Stratigraphic evidence for multiple drainings of glacial Lake Missoula along the Clark Fork River, Montana, USA: Quaternary Research, v. 66, i. 2, p. 311-322.

Smith L., Sohbati, R., Jain, M., 2022, Rock surface luminescence dating of gravel determines the age of a glacial outburst megaflood, Glacial Lake Missoula, Montana, USA: Geology, v. 51, i. 4, p. 323-328.

Smith, 2004, Late Plesitocene stratigraphy and implications for deglaciation and subglacial processes of the Flathead Lobe of the Cordilleran Ice Sheet, Flathead Valley, Montana, USA: *Sedimentary Geology*, v. 165, p. 295-332.

Smith, L., Sohbati, R., Buyalert, J., Lian, O., Murray, A., Jian, M., 2018, Timing of lake-level changes for a deep last-glacial Lake Missoula: optical dating of the Garden Gulch area, Montana, USA: Quaternary Science Reviews, v. 183, p. 13-35.

Softa, M., Spencer, J.Q.G., Sözbilir, H., Huot, S., Emre, T., 2021, Luminescence dating of Quaternary marine terraces from the costal part of Eastern Black Sea and their tectonic implications for the Eastern Pontides, Turkey: *Turkish Journal of Earth Sciences*, v. 30, p. 359-378.

Spencer, J.Q., and Owen, L.A., 2004, Optically stimulated luminescence dating of Late Quaternary glaciogenic sediments in the upper Hunza Valley: Quaternary Science Reviews, v. 23, p. 175–191.

Spencer, J.Q.G., Robinson, R.A.J., 2008, Dating alluvial deposits from NW Argentina using luminescence techniques: Problems and Potential: *Geomorphology*, v. 93, p. 144-155.

Spencer, J., Spencer, T., 2019, New Chronological Data on The Furthest Extent of The Southeastern Flathead Lobe of The Cordilleran Ice Sheet From Luminescence Studies Of Glacio-Deltaic And Moraine Deposits, Flathead Valley, Montana: Geological Society of America Abstracts with Programs, v. 51, n. 5.

Taylor, C., Robinson, T.R., Dunning, S., Carr, J.R., Westoby, M., 2023, Glacial lake outburst floods threaten millions globally: *Nature*, v. 14, i. 487, p. 1-10.

Thomsen, K.J., Jain, M., Murray, A.S., Denby, P.M., Bøtter-Jensen, L., 2008, Minimizing feldspar OSL contamination in quartz UV-OSL using pulsed blue stimulation: Radiation Measurements, v. 43, i. 2-6, p. 752-757.

Thrasher, I., Mauz, B., Chiverrell, R., Lang , A., 2009, Luminescence dating of glaciofluvial deposits: A review: Earth Science Reviews, v. 97, p. 133-146.

Tsakalos, E., Lin, A., Kazantzaki, M., Bassiakos, Y., Nishiwaki, T., Filippaki, E., 2020, Absolute Dating of Past Seismic Events Using the OSL Technique on Fault Gouge Material-A Case Study of the Nojima Fault Zone, SW Japan: Journal of Geophysical Research: Solid Earth, v. 125, p. 1-18.

Tsukamoto, S., Murray, A.S., Huot, S., Watanuki, T., Denby, P.M., Bøtter-Jensen, L., 2007, Luminescnece property of volcanic quartz and the use of red isothermal TL for dating tephras: *Radiation Measurements*, v. 42, p. 190-197.

Waitt Jr., R. B., 1980, About Forty Last-Glacial lake Missoula Jökulhlaups Through Southern Washington: *Journal of Geology,* v. 88, p. 653-679.

Waltham T., 2010, Lake Missoula and the Scablands, Washington, USA: Geology Today, v. 26, i. 4, p. 152-158.

Wintle, A.G., 1997, Luminescence dating: laboratory procedures and protocols: Radiation Measurements, v. 27, i. 5, p. 769-817.

Wintle, A.G., and Murray, A.S., 2006, A review of quartz optically stimulated luminescence characteristics and their relevance in single-aliquot regeneration dating protocols: Radiation Measurements, v. 41, p. 369-391.

Zhu, J., Otto-Bliesner, B.L., brady, E.C., Gettleman, A., Bacmeister, R.B., Poulsen, C.J., Shaw, J.K., McGraw, Z.S., Kay, J.E., 2022, LGM Paleoclimate Constraints Inform Cloud Parametrizations and Equilibrium Climate Sensitivity in CESM2: *Journal of Advances in Modeling Earth*, v. 14, p. 1-18.